processes

MDPI

Review

Review of Two-Dimensional MXenes ($Ti_3C_2T_x$) Materials in Photocatalytic Applications

Haidong Yu [1], Haibing Jiang [1,*], Shuji Zhang [1], Xin Feng [1], Song Yin [1] and Wenzhi Zhao [2]

[1] Langfang Natural Resources Comprehensive Survey Center, China Geological Survey, Langfang 065000, China; yuhaidong1992@163.com (H.Y.); zsj19980526n@163.com (S.Z.); fengxin01305105@163.com (X.F.); syin9614@163.com (S.Y.)
[2] Harbin Natural Resources Comprehensive Survey Center, China Geological Survey, Harbin 150039, China; zhaowenzhi817@163.com
* Correspondence: haib_jiang@126.com

Abstract: MXenes ($Ti_3C_2T_x$) have gotten a lot of interest since their discovery in 2011 because of their distinctive two-dimensional layered structure, high conductivity, and rich surface functional groups. According to the findings, MXenes ($Ti_3C_2T_x$) may block photogenerated electron-hole recombination in the photocatalytic system and offer many activation reaction sites, enhancing the photocatalytic performance and demonstrating tremendous promise in the field of photocatalysis. This review discusses current $Ti_3C_2T_x$-based photocatalyst preparation techniques, such as ultrasonic mixing, electrostatic self-assembly, hydrothermal preparation, and calcination techniques. We also summarised the advancements in photocatalytic CO_2 reduction, photocatalytic nitrogen fixation, photocatalytic hydrogen evolution, and $Ti_3C_2T_x$-based photocatalysts in photocatalytic degradation of pollutants. Lastly, the challenges and prospects of $Ti_3C_2T_x$ in photocatalysis are discussed based on the practical application of $Ti_3C_2T_x$.

Keywords: MXenes material; photocatalysis; preparation method; cocatalyst

check for updates

Citation: Yu, H.; Jiang, H.; Zhang, S.; Feng, X.; Yin, S.; Zhao, W. Review of Two-Dimensional MXenes ($Ti_3C_2T_x$) Materials in Photocatalytic Applications. *Processes* **2023**, *11*, 1413. https://doi.org/10.3390/pr11051413

Academic Editor: Zois Syrgiannis

Received: 22 March 2023
Revised: 22 April 2023
Accepted: 28 April 2023
Published: 6 May 2023

1. Introduction

The study of 2D nanomaterials has grown in popularity since the discovery of graphene in 2004 [1,2]. Because of graphene's superior optical and electronic properties, researchers are particularly interested in studying 2D nanomaterials with layered structures and other multifunctional characteristics, such as transition metal disulfides (MoS_2, WS_2) [3,4], g-C_3N_4 [5,6], layered double hydroxides (LDHs) [7,8], etc. Additionally, this 2D structure can significantly reduce the migration distance between the carrier and the reaction interface, prevent the recombination of holes and photogenerated electrons, and enhance photocatalytic performance [9]. In recent years, MXenes have recently become one of the most popular 2D nanomaterials due to their diversified element composition, distinctive 2D structure, wide surface area, rich surface terminal groups, and good photoelectron characteristics [10–15]. $M_{n+1}X_nT_x$ (MXenes) is a 2D layered structure material obtained by etching $M_{n+1}AX_n$ (n = 1–3) phase, where M represents a transition metal (such as Ti, Nb, V, Ta and Mo), A represents the third and fourth main group elements (such as Si, Ga and Al) in the periodic table, X represents carbon or nitrogen, and T represents its surface functional groups, such as -O, -F, -OH, etc. As shown in Figure 1, more than 50 MXenes have been experimentally synthesized since the discovery of $Ti_3C_2T_x$ MXene in 2011 [16]. $Ti_3C_2T_x$ has emerged as the most extensively utilized MXenes material out of the several MXenes materials identified due to its reasonably established preparation conditions.

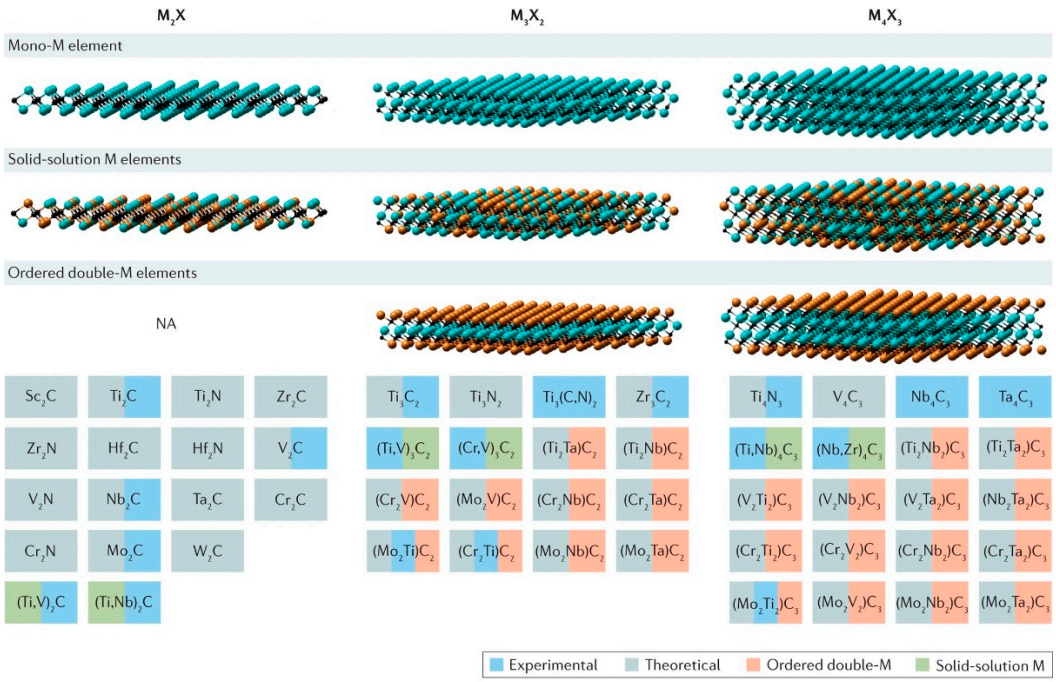

Figure 1. 2D MXenes material that has been reported [17].

2D $Ti_3C_2T_x$ MXenes materials demonstrate that they can produce stronger and larger contact between the bulk phases and semiconductors, which often results in low conjunction at the interface, compared to other 2D layer materials (such as graphene and g-C_3N_4). The separation of charge carriers might be severely limited by the lower and weaker conjunction [18]. Graphene's oxidation will reduce its electronic conductivity and make carrier transfer less reliable, and the reduction process may interfere with certain of its electronic features [19]. However, $Ti_3C_2T_x$ MXenes can easily get over these issues.

There are many methods of synthesis of MXene materials. Direct HF etching and indirect in situ HF etching, which combine HCl and LiF, are the processes most frequently employed to create MXenes [20,21]. In addition, high-temperature etching, chemical vapor deposition, molten-salt etching, and delamination with different organic intercalants (such as dimethyl sulfoxide [22], isopropylamine [23], and tetramethylammonium hydroxide [24]) have also been investigated to increase the production of MXenes. For multilayered MXenes, the primary method is HF and sometimes the delamination with intercalants; however, for delaminated MXenes, the most popular method is MILD etching. Figure 2 shows the chronology of MXenes produced using different etching techniques [25]. $Ti_3C_2T_x$ materials have been widely used in research fields such as supercapacitors, gas sensors and electrocatalysts. In addition to the above applications, in recent years, $Ti_3C_2T_x$ materials as co-catalysts or precursors have also set off a huge research upsurge in the field of photocatalytic environmental remediation and energy conversion. The single-layer $Ti_3C_2T_x$ MXenes material offers the following benefits over the multi-layer $Ti_3C_2T_x$ MXenes material: 1. It might expose more active spots since it has a bigger surface area; 2. The smaller thickness of the single-layer $Ti_3C_2T_x$ decreases the distance between photoinduced electrons moving to the catalyst's surface, further lowering the combinative ratio of charge carriers, and enhancing the photocatalytic performance [26]. 3. Since water molecules may easily absorb on the surface of the single-layer $Ti_3C_2T_x$ material due to its high waterproofness, photocatalytic hydrogen generation can occur more effectively.

Little research has been conducted on the application of $Ti_3C_2T_x$-based photocatalysts in photocatalysis. However, a few reviews have been published on the synthesis and use of $Ti_3C_2T_x$ materials thus far. Therefore, the most recent preparation and application advances of $Ti_3C_2T_x$-based photocatalysts in photocatalysis are discussed in this work to better understand the use of $Ti_3C_2T_x$ materials in the field of photocatalytic environmental

remediation and energy conversion. This review first introduces the synthesis methods of $Ti_3C_2T_x$-based photocatalysts and then systematically reviews recent research on the environmental and energy applications of $Ti_3C_2T_x$-based photocatalysts, such as photocatalytic degradation of organic pollutants, photocatalytic hydrogen evolution, photocatalytic reduction of CO_2, and photocatalytic nitrogen fixation. Finally, the issues raised by using $Ti_3C_2T_x$ materials in photocatalytic environmental remediation and energy science are examined, as are the opportunities for future study.

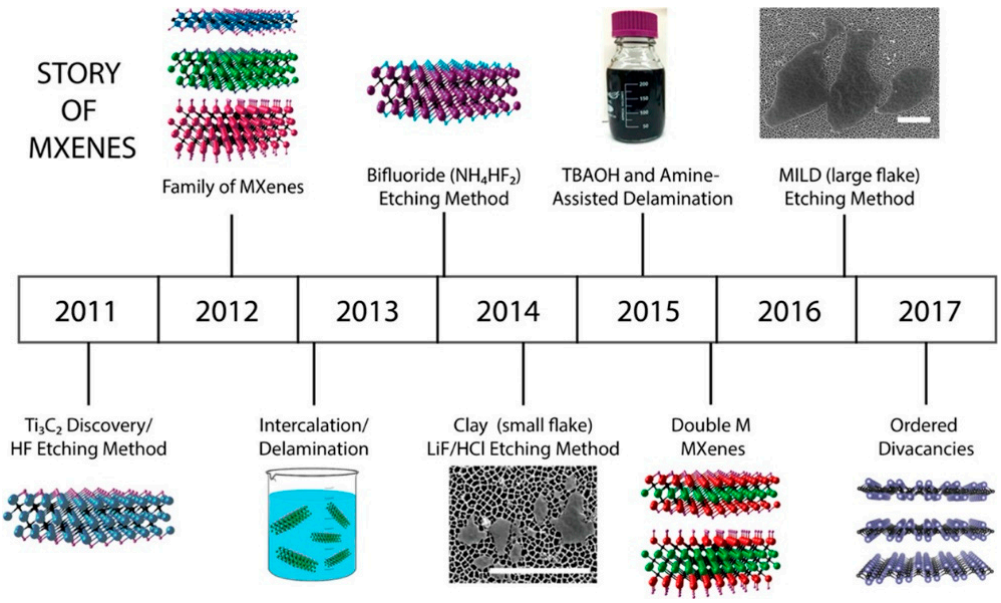

Figure 2. Timeline of MXene etching techniques since Gogotsi's team discovered Ti_3C_2 for the first time in 2011 [25].

2. Synthesis of $Ti_3C_2T_x$-Based Photocatalysts

In recent years, one of the most successful approaches to manufacturing high-efficiency photocatalysts has been the fabrication of composite materials. $Ti_3C_2T_x$ is an attractive study item in photocatalyst preparation due to its unique properties. Mechanical/ultrasonic mixing, electrostatic self-assembly, calcination, and hydrothermal/solvothermal treatment are the most generally utilized procedures for producing $Ti_3C_2T_x$-based photocatalysts.

2.1. Mechanical/Ultrasonic Mixing

The mechanical/ultrasonic mixing method is the most basic and widely used method for producing $Ti_3C_2T_x$-based photocatalysts. To maintain intimate contact between $Ti_3C_2T_x$ and the photocatalyst interface, the synthesis method of intense mechanical stirring or high-power ultrasonic vibration is typically used [27]. Liu et al. [28] produced a $Ti_3C_2T_x$/g-C_3N_4 composite by ultrasonic, centrifugation, and drying after combining g-C_3N_4 aqueous solution with $Ti_3C_2T_x$ aqueous solution, as shown in Figure 3a. The 2D layered structure of $Ti_3C_2T_x$/g-C_3N_4 did not change appreciably when varied quantities of $Ti_3C_2T_x$ and g-C_3N_4 were combined. Similarly, Tahir et al. [29] used an ultrasonic technique to create g-C_3N_4/Bt/$Ti_3C_2T_x$ photocatalyst composites. They began by combining the g-C_3N_4 solution with the Bt suspension. The g-C_3N_4/Bt mixture was then treated with a small quantity of $Ti_3C_2T_x$ while vigorously stirred. The precipitate produced after centrifugation was dried at 100 °C for 24 h after being ultrasonically treated for 60 min. The entire procedure is depicted in Figure 3b. The foregoing studies show that following mechanical/ultrasonic mixing treatments, the contact surfaces of 2D g-C_3N_4 and 2D $Ti_3C_2T_x$ may be intimately connected.

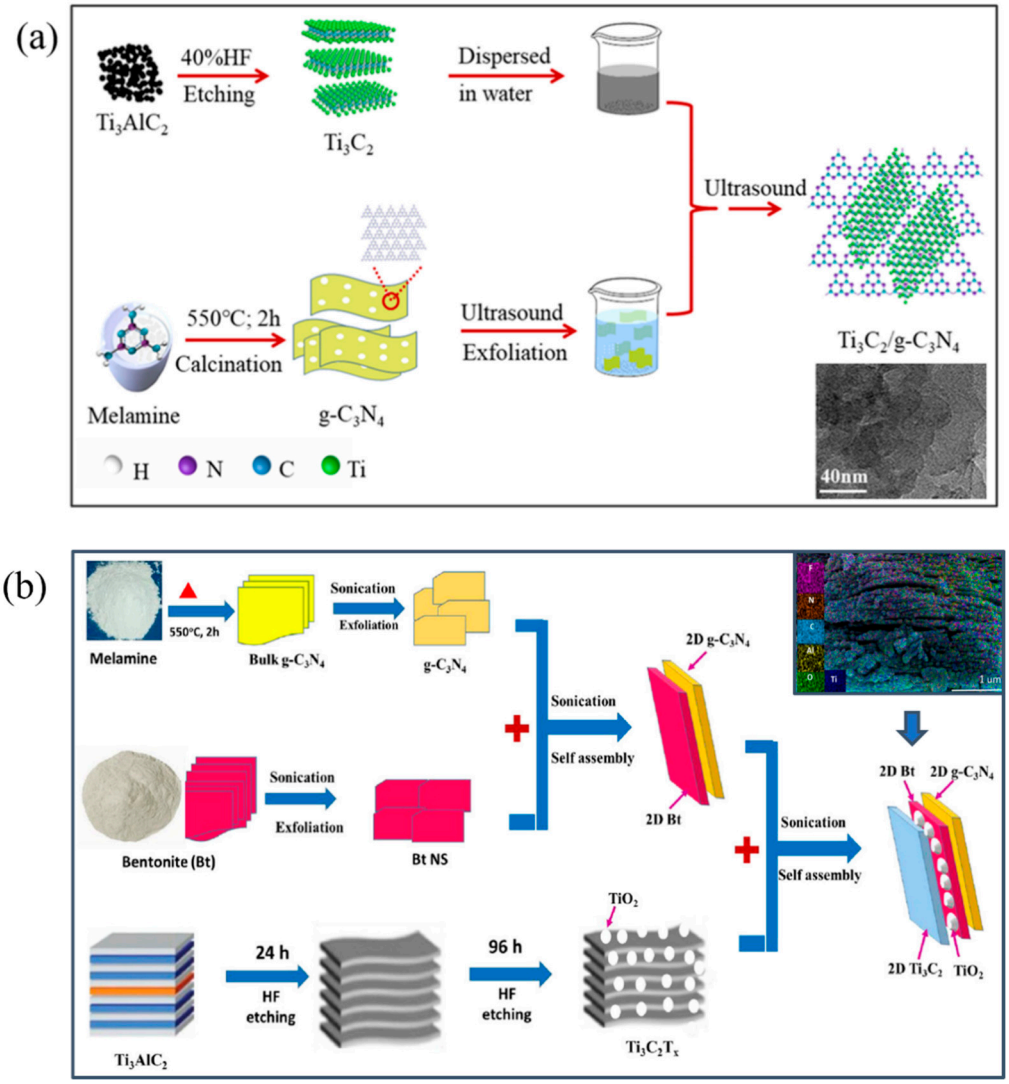

Figure 3. Synthesis process of $Ti_3C_2T_x/g\text{-}C_3N_4$ photocatalyst and TEM pattern of $Ti_3C_2T_x/g\text{-}C_3N_4$ [28] (**a**), Synthesis process of $g\text{-}C_3N_4/Bt/Ti_3C_2T_x$ photocatalyst [29] (**b**).

2.2. Electrostatic Self-Assembly

Electrostatic self-assembly combines two oppositely charged solutes to produce a single or multilayer film on a substrate. The surface of the $Ti_3C_2T_x$ material is heavily charged with negative charges. Constructing with positively charged semiconductors via electrostatic interaction is simple, resulting in 0D/2D, 1D/2D, or 2D/2D $Ti_3C_2T_x$-based photocatalysts. Because monolayer $Ti_3C_2T_x$ materials are particularly prone to agglomeration, ultrasonic treatment is frequently required prior to mixing. For example, Zheng et al. [30] sonicated 0D $Cd_xZn_{1-x}S$ (CZS) with 2D $Ti_3C_2T_x$, and the potential of CZS was +29.6 mV, whereas $Ti_3C_2T_x$ nanosheets had a potential of −22 mV. The $CZS/Ti_3C_2T_x$ composite is created due to the electrostatic attraction between the positively charged CZS nanoparticles and the negatively charged $Ti_3C_2T_x$ nanoparticles, as illustrated in Figure 4a. The picture also shows that CZS nanoparticles are evenly distributed over the surface of $Ti_3C_2T_x$ nanosheets. Li et al. [31] recently synthesized the 1D/2D $CdS/Ti_3C_2T_x$ composites in Figure 4b using an electrostatic self-assembly technique. By electrostatic attraction, $Ti_3C_2T_x$ nanosheets and CdS nanowires may create a strong link, and the CdS nanowires are evenly dispersed throughout the $Ti_3C_2T_x$ nanosheets.

The fabrication of 2D/2D structured photocatalysts has gained increasing interest in recent years. 2D/2D structures possess a bigger contact area and tighter interface contact than 0D/2D and 1D/2D structures, which can increase the effective utilization

of photogenerated electrons and holes [32]. Employing a two-step electrostatic assembly approach, Sharma et al. [33] created a novel 2D-2D-2D ZnO-Bi_2WO_6-$Ti_3C_2T_x$ ternary nanocomposite photocatalyst material made of ZnO, Bi_2WO_6, and $Ti_3C_2T_x$. The interface between the three components contacts and establishes a heterojunction structure, which is favorable to preventing the recombination of photogenerated carriers, as can be shown in Figure 4c.

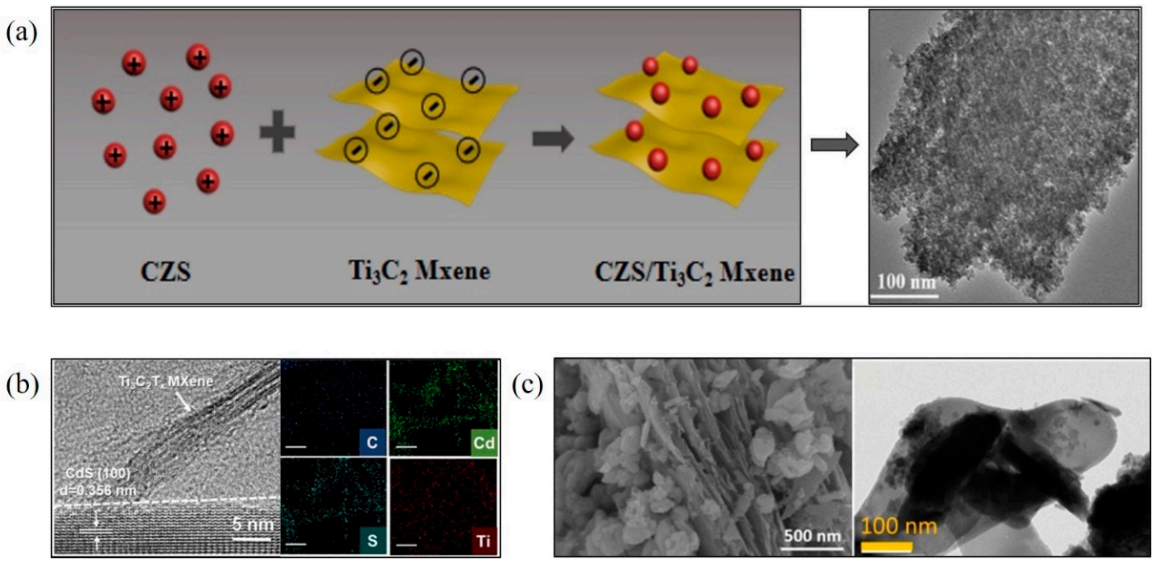

Figure 4. Preparation mechanism and TEM pattern of CZS/$Ti_3C_2T_x$ [30] (**a**), HRTEM image of the binary CdS/$Ti_3C_2T_x$ composite and corresponding elemental mapping images [31] (**b**), SEM and TEM patterns of ZnO-Bi_2WO_6-$Ti_3C_2T_x$ [33] (**c**).

2.3. Calcination

For the production of various g-C_3N_4/$Ti_3C_2T_x$-based photocatalysts, calcination is a heat treatment technique carried out in a temperature–controlled environment. It is generally known that MXenes ($Ti_3C_2T_x$) materials are quickly oxidized in an atmosphere with high temperatures and oxygen. Therefore, N_2 is required as the protective gas for the MXenes-based photocatalyst created via calcination. By calcining a combination of multi-layer $Ti_3C_2T_x$ and urea, Yang et al. [34] also created $Ti_3C_2T_x$/g-C_3N_4 composites and built a 2D/2D heterostructure. According to the research above, the combination of urea and $Ti_3C_2T_x$ that is calcined in a single step is advantageous for further stripping the accordion $Ti_3C_2T_x$. Recently, Zhou et al. [35] designed low-temperature calcination composites of g-C_3N_4, $Ti_3C_2T_x$, and $MoSe_2$. They effectively construct CXM heterojunction by grinding, combining, and calcining ultra-thin $Ti_3C_2T_x$, g-C_3N_4, and $MoSe_2$ at 400 °C for two hours (Figure 5c,d). Strong interface contact between two-dimensional materials may be established by this heterojunction, increasing the separation effect of photogenerated carriers [36].

In addition, other non-$Ti_3C_2T_x$ MXenes photocatalysts have also been obtained through calcination. For example, Wan et al. [37] prepared g-C_3N_4/Mo_2CT_x photocatalyst composite by calcining the mixture of Mo_2CT_x and urea in one step. During the calcination process, urea can release ammonia gas to peel off the multi-layer Mo_2CT_x further and generate g-C_3N_4 on the surface in situ (Figure 5a,b). This calcination method avoids the tedious ultrasonic stripping process of Mo_2CT_x and greatly improves the yield of ultra-thin Mo_2CT_x.

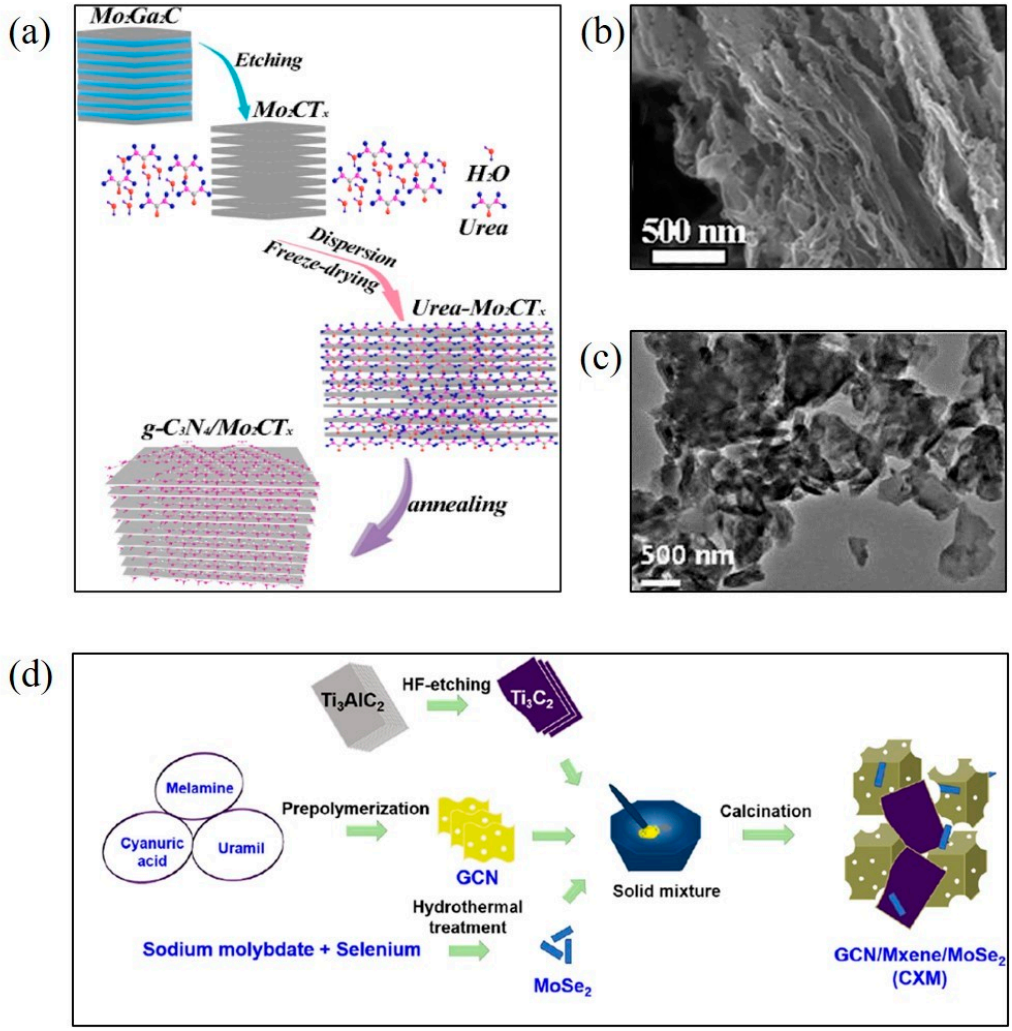

Figure 5. Preparation mechanism (**a**), SEM pattern of g-C_3N_4/Mo_2CT_x [37] (**b**), TEM pattern (**c**), preparation mechanism of CXM [35] (**d**).

2.4. Hydrothermal/Solvothermal

The hydrothermal/solvothermal process allows synthesising composites with high crystallinity and predictable shape since it is carried out in a confined container at high temperature and pressure. Recently, the hydrothermal approach has been used to create several $Ti_3C_2T_x$-based photocatalysts. For instance, the hydrothermal technique was used by Zou et al. [38] to synthesize $MoS_2/Ti_3C_2T_x$ composite. It is evident from Figure 6a that the Schottky heterojunction is formed by the uniform distribution of the crystal MoS_2 phase on the $Ti_3C_2T_x$ layer. Creating 2D/2D MXene matrix composites has also often employed the hydrothermal/solvothermal process. For example, Chen et al. [39] adopted the solvothermal approach to creating 2D/2D $CdS/Ti_3C_2T_x$ composites. The creation of a 2D/2D heterojunction is clearly shown in Figure 6b by the distinguishable interface between $Ti_3C_2T_x$ and CdS.

The hydrothermal/solvothermal method has also been used to obtain other non-$Ti_3C_2T_x$ MXenes photocatalytic compounds. Using an in-situ metal ion derivation method, Cui et al. [40] synthesized 2D/2D Bi_2WO_6/Nb_2CT_x composites. To create 2D/2D Bi_2WO_6/Nb_2CT_x composites, Bi^{2+} was adsorbed onto the surface of Nb_2CT_x during the synthesis and then combined with an aqueous solution of $Na_2WO_4{\cdot}2H_2O$ containing a tiny quantity of CTAB. This reaction took place for 24 h at 120 °C. Figure 6c depicts the mechanism of synthesis as can be observed in Figure 6c, a 2D Bi_2WO_6 and a 2D Nb_2CT_x nano slice success-

fully combined to produce a Schottky circuit, which effectively prevents the recombination of electrons and holes.

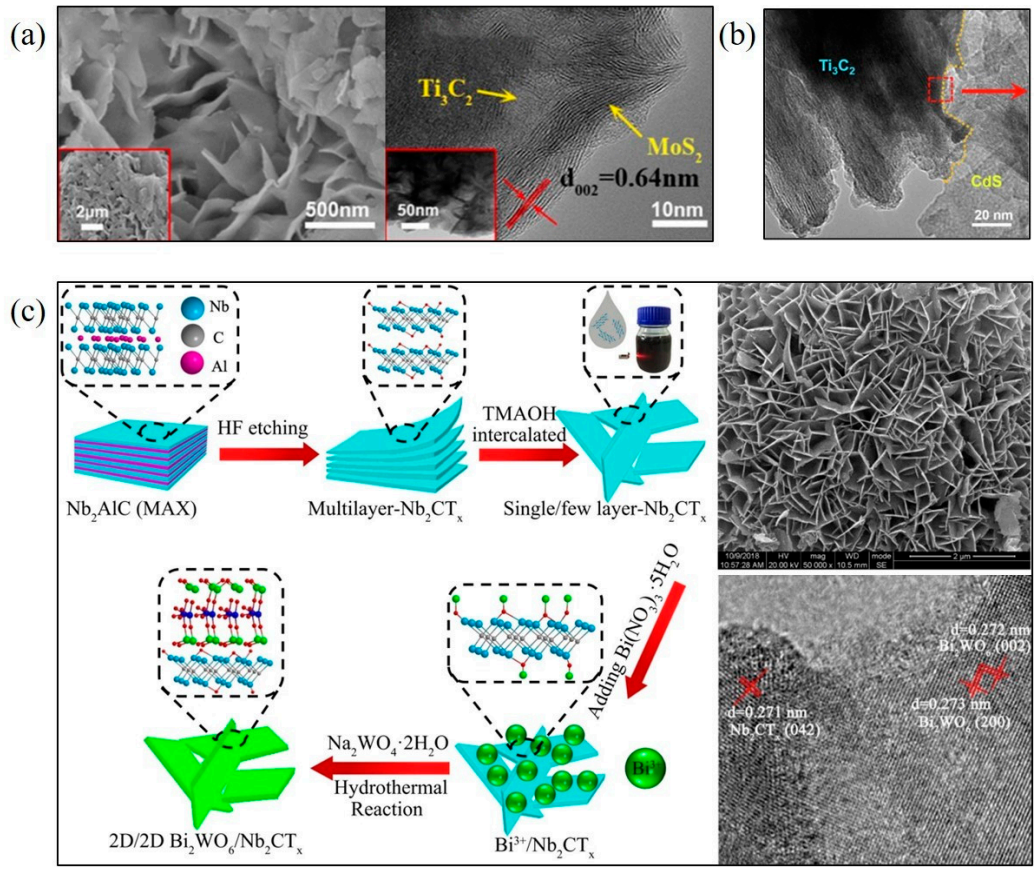

Figure 6. SEM and TEM patterns of $MoS_2/Ti_3C_2T_x$ photocatalysts [38] (**a**), TEM patterns of $CdS/Ti_3C_2T_x$ photocatalysts [39] (**b**), Synthesis mechanism, SEM and TEM patterns of Bi_2WO_6/Nb_2CT_x photocatalyst [40] (**c**).

2.5. Other Methods

High-energy ball milling and wet chemical oxidation are also employed to create $Ti_3C_2T_x$-based photocatalysts in addition to calcination oxidation and hydrothermal oxidation. For instance, Li et al. [41] generated TiO_2-C composites by high-energy ball milling using $Ti_3C_2T_x$ as a precursor (Figure 7a). TiO_2-C nanoflakes have strong photocatalytic activity because titanium dioxide nanoparticles are uniformly and firmly scattered over amorphous carbon, resulting in intimate contact between titanium dioxide and carbon. However, the dotted line in the illustration illustrates that titanium dioxide nanoparticles also have some surface flaws. Some of these structural flaws are brought on by the process of stripping Ti_2AlC using high-energy ball milling [42], and another portion is brought on by the fracture of the original structure brought on by the activation of a few electrons in the titanium dioxide lattice by the mechanical force of ball milling. These flaws enable the development and nucleation of titanium dioxide when Ti_2CT_x is oxidized to TiO_2 during high-energy ball milling [43]. In conclusion, the high-energy ball milling technique has a tight relationship to the structure and characteristics of the TiO_2-C composites that have been created.

It is generally recognized that a photocatalyst's micro-morphology can affect how effectively it performs as a photocatalyst. Through a series of processes, including hydrothermal oxidation, ion exchange, and heat treatment, Tran et al. [44] created the safflower-shaped $TiO_2/Ti_3C_2T_x$ heterostructure (Figure 7b). A 2D $Ti_3C_2T_x$ thin sheet's layered structure is broken down into nanoparticles after hydrothermal treatment and ion exchange. They

discovered that after heating the agglomerated nanoparticles, nanorods began to grow radially from the nanoparticles, eventually forming a composite that appeared like a bit of safflower. The recombination of photogenerated carriers may be successfully prevented by this special nano-flower structure, which promotes charge transfer.

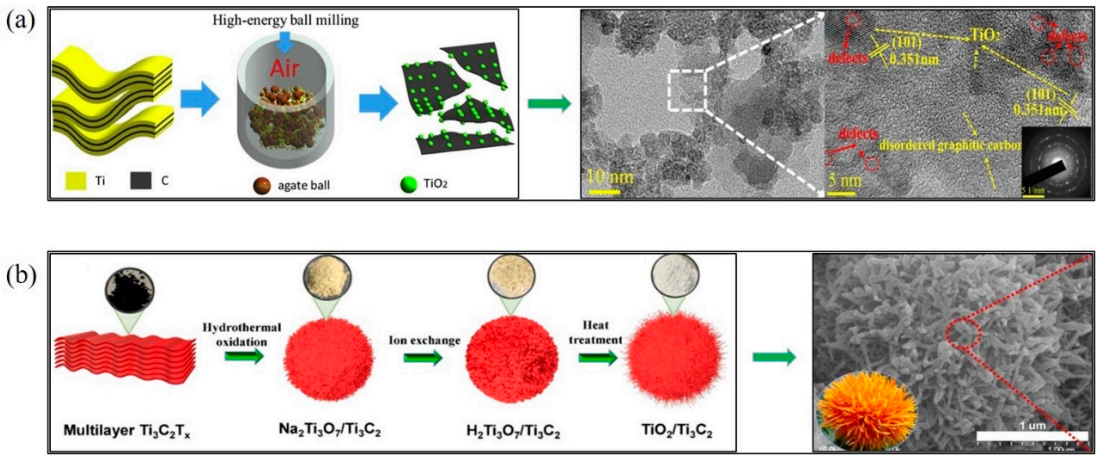

Figure 7. Synthesis mechanism and TEM pattern of TiO_2-C by high-energy ball milling [41] (**a**), Synthesis mechanism and SEM pattern of safflower-like $TiO_2/Ti_3C_2T_x$ photocatalyst [44] (**b**).

3. MXenes ($Ti_3C_2T_x$) Materials for Photocatalytic Applications

3.1. Photocatalytic Degradation of Pollutants

Numerous water resources are being contaminated by organic chemicals due to the quick expansion of contemporary industry and the acceleration of urbanization, with irreparable harm to human health and the environment. As a result, there is a lot of worry about the remediation of water pollution. Adsorption, biological treatment, peroxymonosulfate activation, Fenton oxidation, photocatalysis, and other techniques have all been used in recent years to reduce contaminants in water [45–47]. Among them, photocatalysis is a simple and evident method of photooxidation and photoreduction technology degradation, with carbon dioxide and water as the end products [48,49].

Among the different photocatalysts that may efficiently degrade organic pollutants, $Ti_3C_2T_x$-based photocatalysts have recently emerged as a research hotspot. Furthermore, several investigations have demonstrated the potential of composite materials made of metallic $Ti_3C_2T_x$ and other semiconductor photocatalysts to degrade various contaminants [50]. Wang et al. [51], for instance. Using a hydrothermal technique aided by ultrasound, 2D/2D $Ti_3C_2T_x/SnNb_2O_6$ composites with interfacial Schottky connections were created. When used to photo-catalytically degrade rhodamine B (RhB), $Ti_3C_2T_x/SnNb_2O_6$ showed good results (Figure 8a).

Regarding the shape and structure of composite materials, 2D/2D heterostructures exhibit greater photocatalytic activity than 0D/2D and 1D/2D heterostructures under the same circumstances. This is because 2D/2D heterostructures maximize the area of contact between the two materials while simultaneously offering additional surface reaction activation sites for photocatalysis. Furthermore, since $Ti_3C_2T_x$ has a lower escape work than $SnNb_2O_6$, electrons will flow from it to that material until equilibrium, establishing a potential barrier at the interface that considerably aids in separating photogenerated electrons and holes. Recently, Shao et al. [52] discovered that 2D/2D CoAl-LDHs/$Ti_3C_2T_x$ nanocomposites had a favorable impact on the breakdown of tetracycline hydrochloride (TCH) (Figure 8b). Furthermore, the photocatalytic activity is outstanding due to the synergistic interaction between CoAl-LDHs and $Ti_3C_2T_x$ and the Schottky junction generated on its contact surface (Figure 8c).

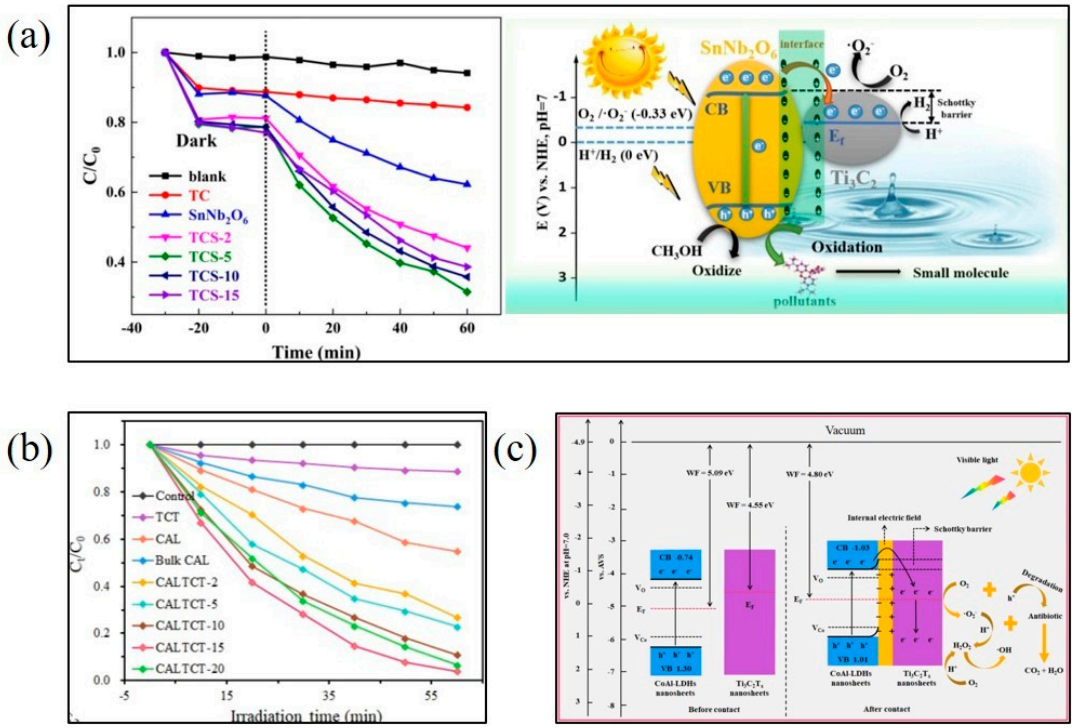

Figure 8. Degradation effect and degradation mechanism of $Ti_3C_2T_x/SnNb_2O_6$ photocatalyst on RhB [51] (**a**), Degradation effect of CoAl-LDHs/$Ti_3C_2T_x$ photocatalyst on TCH [52] (**b**), Degradation mechanism of TCH by CoAl-LDHs/$Ti_3C_2T_x$ photocatalysts [52] (**c**).

3.2. Photocatalytic Hydrogen Evolution

Today, the most significant energy source used worldwide is still fossil fuels. However, our energy use is rising together with the quick growth of human society. Therefore, finding alternative renewable energy sources is so crucial. Because it has cleaner combustion byproducts and a greater energy density than fossil fuels, hydrogen is well known to be a suitable energy source to replace them [53]. Water electrolysis, coal gasification, electrocatalysis, and photocatalysis are now the most widely utilized processes for producing hydrogen [54–66]. However, due to its sustainability and absence of secondary emissions, photocatalytic hydrogen generation is the most promising of these preparation techniques. Numerous types of photocatalysts, including metal sulfide, titanium dioxide, barium titanate, and g-C_3N_4, have been investigated thus far for hydrogen production. However, these photocatalysts still show quick photogenerated carrier recombination and limited light consumption. Therefore, creating novel photocatalysts for hydrogen production by photocatalysis is crucial.

$Ti_3C_2T_x$ has recently been discovered to efficiently separate photogenerated electrons and holes in the field of photocatalytic hydrogen synthesis because of its acceptable Fermi energy level and strong conductivity [67,68]. Therefore, there is a lot of interest in employing $Ti_3C_2T_x$ as electron acceptors and transporters in producing hydrogen via photocatalysis. Using the solvothermal technique, Cao et al. [69] created composites of $Ti_3C_2T_x$ and $Zn_xCd_{1-x}S$ photocatalysts. The experimental results demonstrate that $Ti_3C_2T_x/Zn_xCd_{1-x}S$ has a very good photocatalytic hydrogen evolution effect, up to 14.17 mmol/(h*g), and that this effect is due to the promotion of carrier separation and the enhancement of the oxidation ability of the valence band with a suitable energy band structure (Figure 9a). Meanwhile, it can be seen that $Ti_3C_2T_x/Zn_xCd_{1-x}S$ has good photocatalytic stability, which is due to the introduction of $Ti_3C_2T_x$ to inhibit the photo-corrosion of metal sulfides [70].

It is generally recognized that the photocatalyst's shape significantly impacts how effectively it functions as a catalyst. Due to its two-dimensional ultra-thin structure, two

dimensions, and huge surface area, 2D/2D heterostructure significantly impacts photocatalysis. Based on this assumption, Chen et al. [39] created and produced a special 2D/2D CdS/$Ti_3C_2T_x$ composite photocatalyst with a good photocatalytic hydrogen evolution effect (1.73 mmol/(h*g)) that is higher than that of pure CdS nanoflakes (0.37 mmol/(h*g)) (Figure 9b). This is due to the heterojunction created by the composite of 2D/2D CdS and $Ti_3C_2T_x$, which prevents the quick recombination of photogenerated carriers and encourages the transmission of photogenerated electrons. The above research showed that a $Ti_3C_2T_x$-based photocatalyst could significantly enhance the yield of photocatalytic hydrogen evolution compared with a single semiconductor photocatalyst.

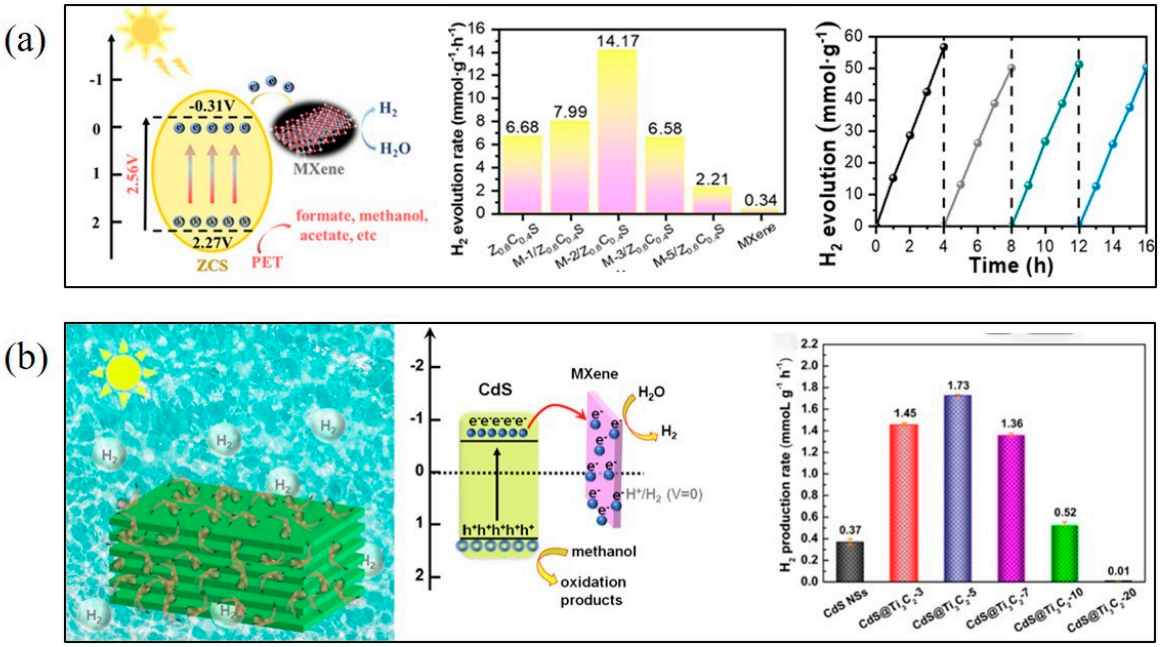

Figure 9. Photocatalytic mechanism, hydrogen evolution and cycle experiment of $Ti_3C_2T_x/Zn_xCd_{1-x}S$ [69] (**a**), 2D/2D CdS/$Ti_3C_2T_x$ photocatalytic mechanism, band structure and photocatalyst hydrogen evolution [39] (**b**).

3.3. Photocatalytic Reduction of CO_2

In recent decades, individuals have made significant efforts in photocatalytic CO_2 reduction to address both the global warming trend and the energy dilemma. The reduction of CO_2 to hydrocarbons (methane, methanol, formaldehyde, formic acid, etc.) and the release of oxygen during photocatalytic CO_2 reduction is a process that mimics the photosynthesis of natural plants. As a result, numerous photocatalysts have been developed and manufactured. However, reducing carbon dioxide by photocatalysts is still difficult because of the interaction of photogenerated carriers, the low thermodynamic stability of carbon dioxide molecules, and the weak adsorption and activation abilities of carbon dioxide molecules [71–74]. Therefore, the development of photocatalysts with strong carbon dioxide reduction activity is urgently needed.

Recently, Li et al. [75] shown that $Ti_3C_2T_x$ may be utilized to construct $Ti_3C_2T_x$/ZnO photocatalyst, which can increase the reduction performance of ZnO photocatalyst to carbon dioxide, and ZnO photocatalyst as a co-catalyst without noble metals. The conversion rate of CO and methane is about seven times and 35 times that of pure ZnO, respectively. The good metal-like conductivity and electron-rich environment of the surface-alkalized $Ti_3C_2T_x$, which favor the separation and transport of photogenerated electrons and holes, are responsible for its higher photocatalytic activity. In addition, the surface terminal -OH group may provide many sites for the adsorption and activation of carbon dioxide molecules. Similarly, Tang et al. [76] employed g-C_3N_4 and alkalized $Ti_3C_2T_x$ as a cocatalyst

to make $Ti_3C_2T_x$-OH/g-C_3N_4. Compared to pure g-C_3N_4, its carbon dioxide photocatalytic reduction increased 5.9 times. According to the study, the -OH terminal groups on the surface of $Ti_3C_2T_x$ may effectively promote the photo-induced transfer of electrons from semiconductors to $Ti_3C_2T_x$-OH (Figure 10). The photocatalytic activity of CO_2 reduction can also be improved by the substantial number of active sites that -OH terminal groups can provide for the adsorption and activation of acidic CO_2 molecules.

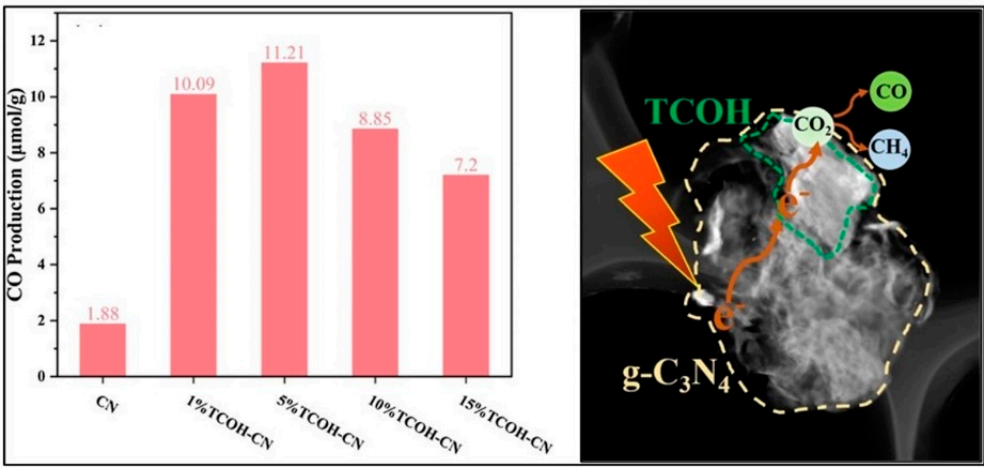

Figure 10. Comparison and mechanism diagram of $Ti_3C_2T_x$-OH/g-C_3N_4 photocatalytic reduction of CO_2 [76].

3.4. Photocatalytic Nitrogen Fixation

As a necessary component of all living things, nitrogen (N) plays a significant role in forming proteins and nucleic acids. The traditional Haber-Bosch method, which currently relies on the reaction of nitrogen and hydrogen to form ammonia at high temperatures and pressures (500–600 °C, 20–50 MPa), is still used to artificially fix nitrogen. However, this process uses a lot of energy and produces a lot of greenhouse gases, which are extremely harmful to the environment. Therefore, the need for a sustainable artificial nitrogen fixation method is important. Photocatalytic technology is one of the most successful ways of artificial nitrogen fixation [77–82]. $Ti_3C_2T_x$ materials have been the subject of much investigation in photocatalytic nitrogen fixation.

$Ti_3C_2T_x$ has enormous promise as a cocatalyst in applying photocatalytic nitrogen fixation. Through experimental investigation and theoretical calculation, Chen et al. [83] recently demonstrated the photocatalytic nitrogen fixation capability of a 2D/2D $Bi_4O_5Br_2$/$Ti_3C_2T_x$ composite. As shown in Figure 11a,b, without using a sacrificial agent, the photocatalyst with a mass ratio of 15% $Ti_3C_2T_x$ has a maximum photocatalytic nitrogen fixation rate of 277.74 μmol/(g*h). $Bi_4O_5Br_2$ and the $Ti_3C_2T_x$ contact form a special ohmic heterojunction that allows electrons to move without a potential barrier. Through an internal electric field, photogenerated electrons may be readily transported from $Bi_4O_5Br_2$ to $Ti_3C_2T_x$.

Furthermore, creating a $Bi_4O_5Br_2/Ti_3C_2T_x$ 2D/2D heterojunction enhances the exposure of active edge sites, shortens the electron transfer path, and increases the efficiency of nitrogen fixation. Similarly, Hou et al. [84] created an in situ $Ti_3C_2T_x/TiO_2$ photocatalyst using a one-step calcination technique and successfully fixed nitrogen by photocatalysis under full-spectrum illumination. As a result, $Ti_3C_2T_x$-based photocatalysts appear to be a potential photocatalytic nitrogen-fixing material because they can create heterojunction via in-situ growth and boost photogenerated carrier separation efficiency.

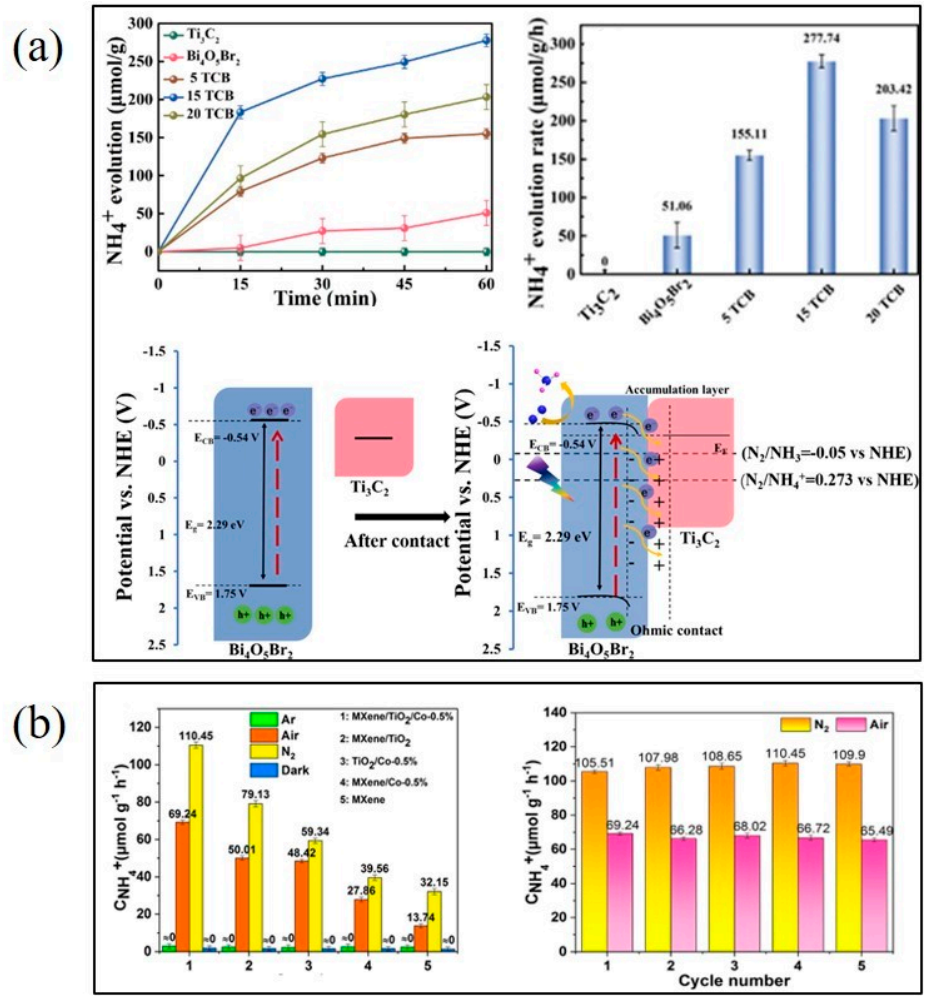

Figure 11. $Bi_4O_5Br_2/Ti_3C_2T_x$ photocatalytic nitrogen fixation curve, nitrogen fixation rate and mechanism diagram [83] (**a**), Experimental diagram of $Ti_3C_2T_x/TiO_2/Co$ photocatalytic nitrogen fixation NH^{4+} [85] (**b**).

3.5. Photocatalytic Applications of $Ti_3C_2T_x$-Derived Materials

Two-dimensional metal carbonates are regarded as good precursors of synthetic composites, whereas the use of $Ti_3C_2T_x$ derivative photocatalysts in the field of photocatalysts has recently gained significant interest from academics. Recent research has demonstrated that the photocatalytic activity of the system may be increased by mixing two-dimensional $Ti_3C_2T_x$ materials with TiO_2 nanoparticles. For instance, Peng et al. [86] produced a photocatalyst ($TiO_{2(001)}/Ti_3C_2T_x$) generated from $Ti_3C_2T_x$ that exposed the uranium dioxide cut (Figure 12a). Under the same conditions, the removal rate of methyl orange (MO) is significantly higher than that of the particle $TiO_2/Ti_3C_2T_x$, which can effectively inhibit the composition of photogenic electrons and holes, improving the photocatalyst degradation effect of the methyl orange (MO). $TiO_{2(001)}/Ti_3C_2T_x$ exhibits good photocatalyst degradation properties for methyl orange (MO) under ultraviolet light. However, in $TiO_2/Ti_3C_2T_x$, the photogenic electron and hole oxidation restore voltage is lower than before the electron transfer, which somewhat restricts the generation of photo-catalytically active compounds [87]. To address this issue more effectively, a Z-type heterogeneous catalytic system has been investigated. This system fixes the shortcomings of the conventional heterogeneous catalytic system, makes it easier to separate the photon electron from the hole, and maximizes the oxidation-restoration power level of the heterogeneous system [88]. Wu et al. [89] created a triple composite photocatalyst of $TiO_2/Ti_3C_2T_x$/AgI with Z-type

heterogeneous nodes using straightforward solvent, thermal procedures, and co-deposition techniques. As a result, the AgI-TiO_2 Z-type heterogeneous bond may be formed using the $Ti_3C_2T_x$ layer as a load transfer bridge (Figure 12b), and the $TiO_2/Ti_3C_2T_x$/AgI composite material shows effective photocatalytic capabilities for the destruction of TCH.

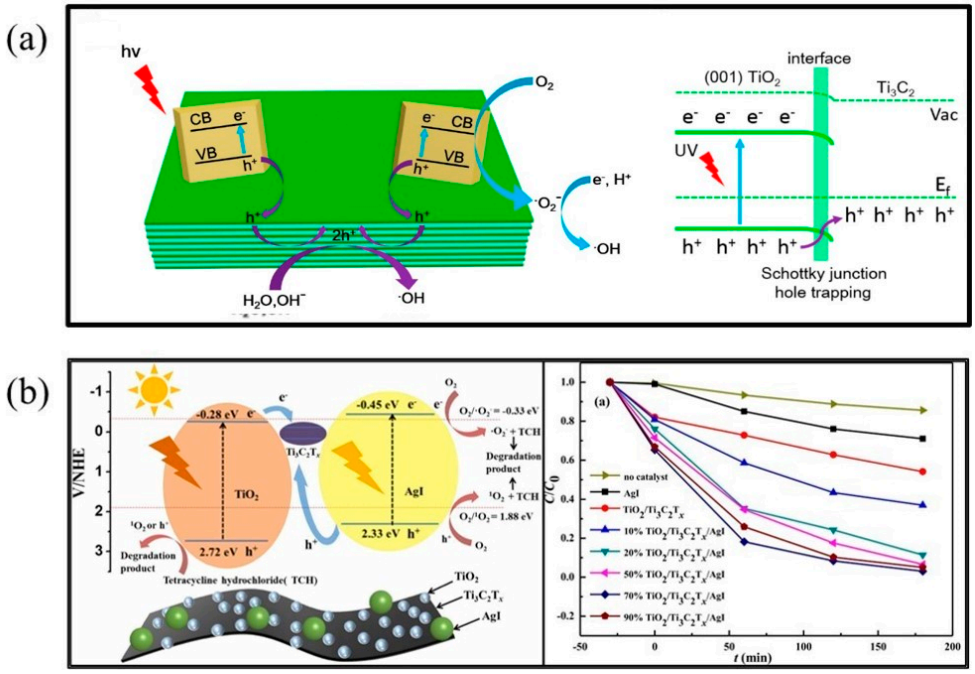

Figure 12. $TiO_2/Ti_3C_2T_x$ band mechanism diagram [86] (**a**), $TiO_2/Ti_3C_2T_x$/AgI band degradation mechanism diagram and degradation curve [89] (**b**).

The $Ti_3C_2T_x$-derived photocatalysts have also sparked a huge research boom in hydrogen evolution. The separation efficiency of photoinduced carriers has been markedly enhanced by the in-situ growth of TiO_2 on the surface of $Ti_3C_2T_x$ when combined with other semiconductors, thus improving photocatalytic hydrogen efficiency [90]. Yang et al. [91] prepared a PtO/$TiO_2/Ti_3C_2T_x$ composite photocatalyst by depositing PtO nanoparticles on the in-situ synthesized $TiO_2/Ti_3C_2T_x$, as shown in Figure 13a, after calcination and oxidation at different time, $Ti_3C_2T_x$ formed $TiO_2/Ti_3C_2T_x$ composites with varying degrees of oxidation. The photocatalytic hydrogen evolution rate was $TiO_2/Ti_3C_2T_x$-12 h > $TiO_2/Ti_3C_2T_x$-20 h > $TiO_2/Ti_3C_2T_x$-4 h, which showed that the increase in titanium dioxide content 12 h before the heating reaction could improve the hydrogen production efficiency. After 12 h, the $Ti_3C_2T_x$ content decreased, resulting in a decrease in hole transfer efficiency, thereby reducing hydrogen evolution efficiency. When PtO nanoparticles are deposited on the surface of $TiO_2/Ti_3C_2T_x$, the hydrogen production efficiency of photocatalysts is significantly increased to 2.54 mmol/(h*g), and $Ti_3C_2T_x$ serves as a hole acceptor for titanium dioxide and PtO in this photocatalyst system, facilitating the separation of photogenerated electrons and holes. Yang et al. [92] used the two-step water thermal location growth method to synthesize the three-dimensional heterogeneous photocatalyst $Ti_3C_2T_x/TiO_2/CuInS_2$ (Figure 13b), and the following factors are primarily responsible for the good photocatalytic effect: 1. Increase the narrow band gap semiconductor $CuInS_2$'s ability to absorb light; 2. Improve charge separation by the synergy of S-type heterojunctions between $CuInS_2$ and TiO_2 and the interface Schottky junction of $Ti_3C_2T_x/CuInS_2$; 3. There are several active areas on the $Ti_3C_2T_x$ surface, which could enhance charge carries separation. Table 1 summarises the photocatalytic H_2 evolution performances of the common $Ti_3C_2T_x$-derived photocatalysts.

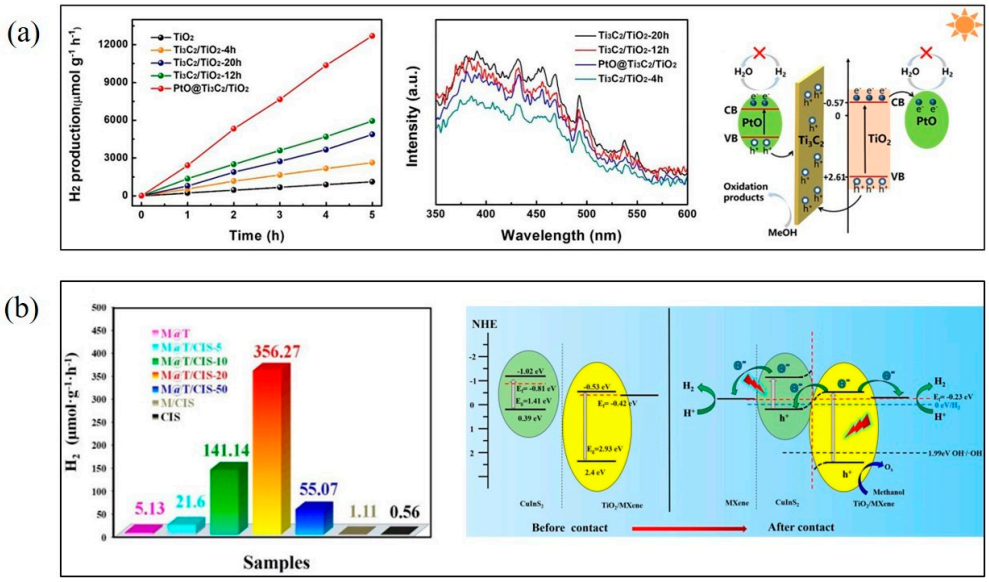

Figure 13. PtO/TiO_2/$Ti_3C_2T_x$ and different calcination times TiO_2/$Ti_3C_2T_x$ hydrogen evolution curves, photoluminescence patterns and mechanism diagrams [91] (**a**) Data and mechanism diagram of hydrogen evolution effect of $Ti_3C_2T_x$/TiO_2/$CuInS_2$ [92] (**b**).

Table 1. Summary of photocatalytic activity of Ti_3C_2/TiO_2 composites for H_2 evolution.

Photocatalysts	Sacrificial Regent	H_2 Production Rate (μmol/(h*g))	Light Source
Ti_3C_2/TiO_2 [93]	Methanol	2650	200 W Hg lamp
Cu_2O/Ti_3C_2/TiO_2 [48]	Methanol	1496	300 W Xenon lamp
Ti_3C_2/TiO_2/UiO-66-NH [90]	Na_2SO_3	1980	300 W Xenon lamp
Ti_3C_2/TiO_2/Ru [94]	Methanol	235.3	300 W Xenon lamp
WS_2/Ti_3C_2/TiO_2 [95]	Triethanolamine	3409.8	300 W Xenon lamp
LDS-S-Ti_3C_2/TiO_2 [96]	Methanol	333	300 W Xenon lamp
Ti_3C_2/TiO_2 (Nanoflowers) [97]	TEOA	526	300 W Xenon lamp
MoS_2/Ti_3C_2/TiO_2 [98]	TEOA	6425.297	300 W Xenon lamp

Hou et al. [84] synthesized $Ti_3C_2T_x$/TiO_2 photocatalyst in situ by one-step calcination technology and achieved a good photocatalytic nitrogen fixation effect under full-spectrum radiation. It can be seen that $Ti_3C_2T_x$-derived photocatalyst can form heterojunctions through in-situ growth, improve the separation efficiency of photogenerated carriers, and is a promising photocatalytic nitrogen fixing material. On this basis, Gao et al. [85] synthesized $Ti_3C_2T_x$/TiO_2/Co by introducing Co into $Ti_3C_2T_x$-derived photocatalysts using a two-step calcination method, which achieved high efficiency and stable photocatalytic nitrogen fixation. As shown in Figure 11b, the NH_3 yield without any pore sacrifice was as high as 110.45 μmol/(g*h) under an N_2 environment and UV-visible light. This is attributed to the improvement of carrier transfer and separation by in-situ growth of $Ti_3C_2T_x$/TiO_2 heterojunction by calcination, Co doping effectively regulates the chemical adsorption equilibrium of reactant N_2 and product ammonia on the catalyst surface, and $Ti_3C_2T_x$/TiO_2/Co photocatalysis shows certain cyclic stability due to the presence of $Ti_3C_2T_x$. From the above

experiments, it can be seen that $Ti_3C_2T_x$ has great application prospects in photocatalytic nitrogen fixation.

3.6. Photocatalytic Applications of Non-$Ti_3C_2T_x$ MXenes

Aside from the widespread use of $Ti_3C_2T_x$ materials in photocatalytic applications, some non-$Ti_3C_2T_x$ materials have significantly advanced in photocatalysis in recent years. For example, the new MXene 2D niobium carbide (Nb_2CT_x), which has a lower Fermi level than $Ti_3C_2T_x$, was used as an excellent co-catalyst. Recently, Makola et al. [99] used an in-situ calcination method to prepare a 2D/2D Nb_2CT_x@g-C_3N_4 metal-free Schottky junction photocatalyst with different loading percentages of Nb_2CT_x. The varying quantities of Nb_2CT_x loaded onto the g-C_3N_4 had no discernible effect on the chemical composition and structure. However, due to alterations in band edge locations, the produced heterostructures had narrower energy band gaps than g-C_3N_4.

Furthermore, the development of the Schottky junction, where Nb_2CT_x functions as an electron sink, considerably reduced electron recombination rates. The electrochemical tests revealed that the samples had increased photocatalytic activity following the creation of the heterostructure. The band edge diagram demonstrates good band locations for the composites to be employed in various photocatalytic applications, including CO_2 reduction, photooxidation, and species reduction. To further specific applications, Huang et al. [100] recently demonstrated the photocatalytic hydrogen generation capability of a 1D/2D CdS/Nb_2CT_x MXene composite. The photocatalyst's maximal photocatalytic hydrogen production rate with a purity of 60 mg Nb_2CT_x is 5.3 mmol/(g*h), which is 1.7 times greater than that of pristine CdS. The findings above are due to the special properties of Nb_2CT_X MXene (high conductivity, 2D structure, and enough active sites) and the close interface contact. In the meantime, the CdS/Nb_2CT_X combination can efficiently increase the number of free radicals and the separation and transmission of photoexcited electron-hole pairs. The studies mentioned above can serve as references for the design of non-$Ti_3C_2T_x$ as a co-catalyst for better photocatalytic applications. However, there are currently limited studies on non-$Ti_3C_2T_x$ materials in photocatalysis.

4. Major Properties of $Ti_3C_2T_x$ MXenes Materials in Photocatalysis

4.1. Facilitating the Separation of Photogenerated Electrons and Holes

To address the poor efficiency of photocatalysis, the primary method is to increase the separation efficiency of photogenerated carriers. Using $Ti_3C_2T_x$ as a co-catalyst may generally successfully prevent the recombination of photogenerated electrons and holes in the photocatalytic system because of the material's suitable Fermi energy level and strong electrical conductivity. In addition, numerous experimental findings demonstrate that $Ti_3C_2T_x$ with a semiconductor photocatalyst can produce a heterojunction (ohmic or Schottky contact). The metal-semiconductor Schottky contact will form on the contact surface of the two when the work function of the metal is greater than that of the semiconductor in the n-type semiconductor, and a Schottky barrier can form inside it that can be used as an electron absorber to stop electron backflow [101]. On the other hand, a metal-semiconductor ohmic contact will form on the contact surface of the two when the work function of the metal in an n-type semiconductor is lower than that of the semiconductor [102].

In contrast to Schottky contact, Ohmic contact is not constrained by an energy barrier, allowing photogenerated electrons to move spontaneously from $Ti_3C_2T_x$ to semiconductors until they achieve equilibrium [103]. Furthermore, the kinetics of the photocatalytic reaction may be efficiently accelerated by ohmic contact, increasing the photocatalytic efficiency. In conclusion, the heterojunction structure created by combining semiconductors with $Ti_3C_2T_x$ materials may effectively prevent the recombination of photogenerated carriers, enhancing photocatalytic activity.

4.2. Providing a Large Number of Modifiable Active Sites

The structure and surface characteristics of the material, in addition to the material's inherent features, have a significant influence on the catalytic activity. The two-dimensional planar structure of the $Ti_3C_2T_x$ material not only reduces the transmission distance of the widely produced charge carriers and offers additional surface-active areas for photocatalysis. There are currently two techniques that are often used to produce $Ti_3C_2T_x$ materials. One involves using HF to peel directly, while the other involves using a solution of HCL and LiF to peel indirectly. The two strategies result in distinct terminal groupings. The latter has more -O/-OH terminals than the $Ti_3C_2T_x$ etched using hydrochloric acid or lithium fluoride, which mostly has -F terminals. The photocatalytic process is somewhat influenced by the various end groups. For instance, Ran et al. [104] showed that the photocatalytic hydrogen precipitation rate rose with a decrease in the terminal group -F to -O ionization ratio. However, the result was not particularly satisfactory. The -F exposed to the $Ti_3C_2T_x$ surface renders the external atomic charge saturated since the halogen elements are in group VIIA. From a thermodynamic perspective, the $Ti_3C_2T_x$ surface is highly stable, making it challenging for the externally photoexcited electrons to reach it.

The $Ti_3C_2T_x$ surface is negatively charged due to the -F and -OH terminals from a kinetic perspective, making Coulomb gravity difficult to attract foreign electrons with the same negative charge. At the same time, Li et al. [105] demonstrated through theory and experimentation that $Ti_3C_2T_x$ at the -F and -OH terminals covered up their active surface sites, resulting in their catalytic ammonia production and efficiency for nitrogen fixation. In conclusion, $Ti_3C_2T_x$, functionalized with a non-active group, is unsuitable for a cocatalyst in the photocatalytic reaction. This significantly restricts the application of $Ti_3C_2T_x$ materials in the area of photocatalysis. To address the issues mentioned above, Zhong et al. [106] replaced the passivation groups (-F, -O/-OH) on the $Ti_3C_2T_x$ surface with diamino ethanethiol (AET) using a straightforward sonication process. As a result, they produced surface-modified CdZnS/$Ti_3C_2T_x$-AET nanosheets with high surface activity. The surface-modified CdZnS/$Ti_3C_2T_x$-AET had much better catalytic activity than the original CdZnS and CdZnS/$Ti_3C_2T_x$ and outperformed most of the reported $Ti_3C_2T_x$-based catalysts. Therefore, adding the right functional groups to $Ti_3C_2T_x$ surfaces may significantly increase the interfacial carrier transfer activity, create many active sites, and broaden the use of $Ti_3C_2T_x$ materials in photocatalysis.

4.3. Enhancing Photocatalytic Stability by Inhibiting Anti-Photocorrosion

Various semiconductor photocatalysts for environmental cleaning have been produced, such as $AgNO_3$ and CdS. However, aside from the combination of photoinduced electrons and holes substantially restricting photoactivity, the issues caused by photogenerated holes-induced anti-photocorrosion greatly restrict its practical applicability.

Cai et al. [107] prepared the Ag_3PO_4/Ti_3C_2 MXene Schottky catalyst to solve the above issues via a driven self-assembly approach. It not only has great light degradation capabilities for dye, but it also has superior photocatalytic stability compared to pure Ag_3PO_4. After eight cycles (Figure 14a), the photocatalytic capabilities of pure Ag_3PO_4 reduced by approximately 92.2%, suggesting a larger quantity of breakdown induced by photocorrosion. In contrast, the Ag_3PO_4/Ti_3C_2 composite has a relatively small loss of after-light catalysis performance (about 31.6% in eight cycles), indicating that its anti-photocorrosion is inhibited, which is attributed to a full and tight interface contact between Ag_3PO_4 and Ti_3C_2, a single-directional electron flow captured by Ti_3C_2 through the Schottky barrier, and Ti sites with higher redox reactivity on the surface of Ti_3C_2. Similarly, Xie et al. [70] used Ti_3C_2 as a precursor to create 2D/2D CdS/Ti_3C_2 heterostructures using a simple electrostatic self-assembly technique. CdS/Ti_3C_2 showed high photoactivity for 4-nitroaniline (4-NA) degradation. Meanwhile, Ti_3C_2 inhibited CdS photocorrosion. As shown in Figure 14b, the degradation of 4-NA over pure CdS nanosheets gradually declines, implying that the use of ammonium formate as hole scavengers cannot entirely prevent photocorrosion of CdS. CdS-0.5% MXene, on the other hand, has better stability for 4-NA conversion. The

close connection between CdS nanosheets and $Ti_3C_2T_x$ is advantageous in exerting the "Cd^{2+} confinement effect" of $Ti_3C_2T_x$, hence improving the stability of CdS-based photocatalysts. In summary, introducing Ti can effectively enhance the stability of photocatalyst composite materials.

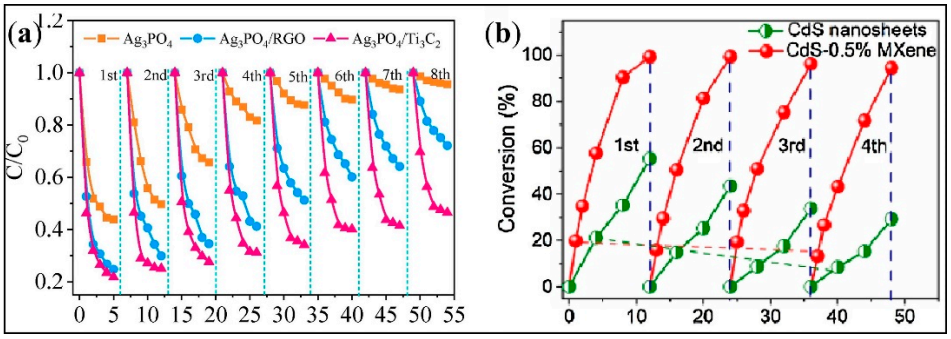

Figure 14. The photocatalytic stability of Ag_3PO_4/Ti_3C_2 composite [107] (**a**), The photocatalytic stability of CdS/Ti_3C_2 composite [70] (**b**).

5. Summary and Outlook

Since $Ti_3C_2T_x$ material initially appeared in 2011, its use in photocatalysis has garnered much interest. The preparation techniques for $Ti_3C_2T_x$-based photocatalysts that are often utilized include mechanical or ultrasonic mixing, electrostatic self-assembly, the water/solvothermal approach, and the calcination method, as discussed in this study. $Ti_3C_2T_x$ is typically used as a cocatalyst in the field of photocatalytic environmental remediation and energy conversion, including organic pollutant degradation, water decomposition for hydrogen production, carbon dioxide reduction, and photocatalytic nitrogen fixation, due to its adjustable element composition, unique 2D layered structure, large surface area, rich surface ends, and good photoelectron properties. Furthermore, theoretical research and numerous tests demonstrate that the semiconductor photocatalyst and $Ti_3C_2T_x$ can create a heterojunction (ohmic contact or Schottky contact), which can successfully facilitate the separation of photogenerated carriers. Additionally, by appropriately altering the many terminal sites on its surface, the photocatalytic efficacy may increase further. However, contrary to studies on other 2D materials, $Ti_3C_2T_x$ is still in its infancy, and several problems need to be resolved before it can be applied broadly.

1. $Ti_3C_2T_x$ is currently synthesized using procedures that are still mostly difficult, time-consuming, and yield-poor. To synthesize $Ti_3C_2T_x$ on a wide scale, it is important to develop an affordable, effective, and ecologically friendly process.
2. MXenes materials have not been thoroughly studied in comparison to $Ti_3C_2T_x$. For instance, there aren't many studies on V_2CT_x, Nb_2CT_x, and the composites they're formed from, such as V_2O_5/V_2CT_x, Nb_2O_5/Nb_2CT_x, etc. Therefore, future research into non-$Ti_3C_2T_x$ MXenes photocatalysts is quite promising. Additionally, V_2CT_x and Nb_2CT_x materials perform better than $Ti_3C_2T_x$ MXenes, which may result in discoveries in the field of photocatalysis.
3. The ease with which $Ti_3C_2T_x$ may oxidize in oxygen-containing environments is widely recognized. However, the $Ti_3C_2T_x$ structure's decomposition will impact the photocatalytic activity. Numerous methods have been suggested thus far to increase the stability of $Ti_3C_2T_x$, such as enhancing the preparation conditions, introducing antioxidants, etc. Photocatalysts based on $Ti_3C_2T_x$ will perform at a higher level in energy and environmental applications if the problem of oxidation resistance can be resolved.

Author Contributions: Conceptualization, H.J.; methodology, H.Y.; software, S.Y.; validation, S.Z.; formal analysis, W.Z.; investigation, H.Y.; resources, X.F.; data curation, S.Y.; writing—original draft preparation, H.J.; writing—review and editing, H.Y.; visualization, X.F.; supervision, S.Z. All authors have read and agreed to the published version of the manuscript.

Funding: This research received no external funding.

Data Availability Statement: Not applicable.

Conflicts of Interest: The authors declare no conflict of interest. The funders had no role in the study's design; in the collection, analyses, or interpretation of data; in the writing of the manuscript; or in the decision to publish the results.

References

1. Novoselov, K.S.; Geim, A.K.; Morozov, S.V.; Jiang, D.; Zhang, Y.; Dubonos, S.V.; Grigorieva, I.V.; Firsov, A.A. Electric field effect in atomically thin carbon films. *Science* **2004**, *306*, 666–669. [CrossRef] [PubMed]
2. Huang, H.; Song, Y.; Li, N.; Chen, D.; Xu, Q.; Li, H.; He, J.; Lu, J. One-step in-situ preparation of N-doped TiO_2@C derived from Ti_3C_2 MXene for enhanced visible-light driven photodegradation. *Appl. Catal. B Environ.* **2019**, *251*, 154–161. [CrossRef]
3. Zhang, L.; Ji, X.; Ren, X.; Ma, Y.; Shi, X.; Tian, Z.; Asiri, A.M.; Chen, L.; Tang, B.; Sun, X. Electrochemical Ammonia Synthesis via Nitrogen Reduction Reaction on a MoS_2 Catalyst: Theoretical and Experimental Studies. *Adv. Mater.* **2018**, *30*, e1800191. [CrossRef] [PubMed]
4. Jin, C.; Regan, E.C.; Yan, A.; Iqbal Bakti Utama, M.; Wang, D.; Zhao, S.; Qin, Y.; Yang, S.; Zheng, Z.; Shi, S.; et al. Observation of moiré excitons in WSe_2/WS_2 heterostructure superlattices. *Nature* **2019**, *567*, 76–80. [CrossRef]
5. Guo, R.-T.; Wang, J.; Bi, Z.-X.; Chen, X.; Hu, X.; Pan, W.-G. Recent advances and perspectives of g-C3N4-based materials for photocatalytic dyes degradation. *Chemosphere* **2022**, *295*, 133834. [CrossRef] [PubMed]
6. Que, M.; Cai, W.; Chen, J.; Zhu, L.; Yang, Y. Recent advances in g-C_3N_4 composites within four types of heterojunctions for photocatalytic CO_2 reduction. *Nanoscale* **2021**, *13*, 6692–6712. [CrossRef]
7. Tan, L.; Wang, Z.; Zhao, Y.; Song, Y.-F. Recent Progress on Nanostructured Layered Double Hydroxides for Visible-Light-Induced Photoreduction of CO_2. *Chem. Asian J.* **2020**, *15*, 3380–3389. [CrossRef] [PubMed]
8. Wang, L.; Zhu, Z.; Wang, F.; Qi, Y.; Zhang, W.; Wang, C. State-of-the-art and prospects of Zn-containing layered double hydroxides (Zn-LDH)-based materials for photocatalytic water remediation. *Chemosphere* **2021**, *278*, 130367. [CrossRef] [PubMed]
9. Wang, K.; Li, J.; Zhang, G. Ag-Bridged Z-Scheme 2D/2D $Bi_5FeTi_3O_{15}$/g-C_3N_4 Heterojunction for Enhanced Photocatalysis: Mediator-Induced Interfacial Charge Transfer and Mechanism Insights. *ACS Appl. Mater. Interfaces* **2019**, *11*, 27686–27696. [CrossRef] [PubMed]
10. Yang, J.; Cheng, S.; Zhang, S.; Han, W.; Jin, B. Modifying Ti_3C_2 MXene with NH^{4+} as an excellent anode material for improving the performance of microbial fuel cells. *Chemosphere* **2022**, *288*, 132502. [CrossRef]
11. Chen, Z.; Asif, M.; Wang, R.; Li, Y.; Zeng, X.; Yao, W.; Sun, Y.; Liao, K. Recent Trends in Synthesis and Applications of porous MXene Assemblies: A Topical Review. *Chem. Rec.* **2021**, *22*, e202100261. [CrossRef] [PubMed]
12. Mu, W.; Du, S.; Li, X.; Yu, Q.; Wei, H.; Yang, Y.; Peng, S. Removal of radioactive palladium based on novel 2D titanium carbides. *Chem. Eng. J.* **2019**, *358*, 283–290. [CrossRef]
13. Im, J.K.; Sohn, E.J.; Kim, S.; Jang, M.; Son, A.; Zoh, K.-D.; Yoon, Y. Review of MXene-based nanocomposites for photocatalysis. *Chemosphere* **2021**, *270*, 129478. [CrossRef]
14. Garg, R.; Agarwal, A.; Agarwal, M. Synthesis and Characterization of Solution Processed MXene. In Proceedings of the 64th DAE Solid State Physics Symposium (DAE-SSPS), Indian Institute of Technology Jodhpur, Jodhpur, India, 18–22 December 2019.
15. Wang, H.; Roeffaers, B.J.; Weng, B.; Wang, Y.; Ji, H. Ultrathin 2D/2D $Ti_3C_2T_x$/semiconductor dual_functional photocatalysts for simultaneous imine production and H_2 evolution. *J. Mater. Chem. A* **2021**, *9*, 19984–19993. [CrossRef]
16. Naguib, M.; Kurtoglu, M.; Presser, V.; Lu, J.; Niu, J.; Heon, M.; Hultman, L.; Gogotsi, Y.; Barsoum, M.W. Two-Dimensional Nanocrystals Produced by Exfoliation of Ti_3AlC_2. *Adv. Mater.* **2011**, *23*, 4248–4253. [CrossRef]
17. Anasori, B.; Lukatskaya, M.R.; Gogotsi, Y. 2D metal carbides and nitrides (MXenes) for energy storage. *Nat. Rev. Mater.* **2017**, *2*, 16098. [CrossRef]
18. Liu, L.; Qi, Y.; Lu, J.; Lin, S.; An, W.; Liang, Y.; Cui, W. A stable Ag_3PO_4@g-C_3N_4 hybrid core@shell composite with enhanced visible light photocatalytic degradation. *Appl. Catal. B Environ.* **2016**, *183*, 133–141. [CrossRef]
19. Hernandez, Y.; Nicolosi, V.; Lotya, M.; Blighe, F.M.; Sun, Z.; De, S.; McGovern, I.T.; Holland, B.; Byrne, M.; Gun'Ko, Y.K.; et al. High-yield production of graphene by liquid-phase exfoliation of graphite. *Nat. Nanotechnol.* **2008**, *3*, 563–568. [CrossRef]
20. Shi, H.; Zhang, P.; Liu, Z.; Park, S.; Lohe, M.R.; Wu, Y.; Shaygan Nia, A.; Yang, S.; Feng, X. Ambient-Stable Two-Dimensional Titanium Carbide (MXene) Enabled by Iodine Etching. *Angew. Chem. Int. Ed.* **2021**, *60*, 8689–8693. [CrossRef]
21. Rakhi, R.B.; Ahmed, B.; Hedhili, M.N.; Anjum, D.H.; Alshareef, H.N. Effect of Postetch Annealing Gas Composition on the Structural and Electrochemical Properties of Ti_2CT_x MXene Electrodes for Supercapacitor Applications. *Chem. Mater.* **2015**, *27*, 5314–5323. [CrossRef]

22. Sun, D.; Wang, M.; Li, Z.; Fan, G.; Fan, L.-Z.; Zhou, A. Two-dimensional Ti_3C_2 as anode material for Li-ion batteries. *Electrochem. Commun.* **2014**, *47*, 80–83. [CrossRef]
23. Rajavel, K.; Shen, S.; Ke, T.; Lin, D. Achieving high bactericidal and antibiofouling activities of 2D titanium carbide ($Ti_3C_2T_x$) by delamination and intercalation. *2D Mater.* **2019**, *6*, 035040. [CrossRef]
24. Xie, Y.; Rahman, M.M.; Kareem, S.; Dong, H.; Qiao, F.; Xiong, W.; Liu, X.; Li, N.; Zhao, X. Facile synthesis of CuS/MXene nanocomposites for efficient photocatalytic hydrogen generation. *CrystEngComm* **2020**, *22*, 2060–2066. [CrossRef]
25. Alhabeb, M.; Maleski, K.; Anasori, B.; Lelyukh, P.; Clark, L.; Sin, S.; Gogotsi, Y. Guidelines for Synthesis and Processing of Two-Dimensional Titanium Carbide ($Ti_3C_2T_x$ MXene). *Chem. Mater.* **2017**, *29*, 7633–7644. [CrossRef]
26. Low, J.; Zhang, L.; Tong, T.; Shen, B.; Yu, J. TiO_2/MXene Ti_3C_2 composite with excellent photocatalytic CO_2 reduction activity. *J. Catal.* **2018**, *361*, 255–266. [CrossRef]
27. Li, Y.; Chen, X.; Sun, Y.; Meng, X.; Dall'Agnese, Y.; Chen, G.; Dall'Agnese, C.; Ren, H.; Sasaki, S.-i.; Tamiaki, H.; et al. Chlorosome-Like Molecular Aggregation of Chlorophyll Derivative on $Ti_3C_2T_x$ MXene Nanosheets for Efficient Noble Metal-Free Photocatalytic Hydrogen Evolution. *Adv. Mater. Interfaces* **2020**, *7*, 1902080. [CrossRef]
28. Liu, W.; Sun, M.; Ding, Z.; Gao, B.; Ding, W. Ti_3C_2 MXene embellished g-C_3N_4 nanosheets for improving photocatalytic redox capacity. *J. Alloys Compd.* **2021**, *877*, 160223. [CrossRef]
29. Tahir, M.; Tahir, B. 2D/2D/2D O-C_3N_4/Bt/$Ti_3C_2T_x$ heterojunction with novel MXene/clay multi-electron mediator for stimulating photo-induced CO_2 reforming to CO and CH_4. *Chem. Eng. J.* **2020**, *400*, 125868. [CrossRef]
30. Zheng, S.; Peng, S.; Wang, Z.; Huang, J.; Luo, X.; Han, L.; Li, X. Schottky-structured 0D/2D composites via electrostatic self-assembly for efficient photocatalytic hydrogen evolution. *Ceram. Int.* **2021**, *47*, 28304–28311. [CrossRef]
31. Li, J.-Y.; Li, Y.-H.; Zhang, F.; Tang, Z.-R.; Xu, Y.-J. Visible-light-driven integrated organic synthesis and hydrogen evolution over 1D/2D CdS-$Ti_3C_2T_x$ MXene composites. *Appl. Catal. B Environ.* **2020**, *269*, 118783. [CrossRef]
32. Zhong, Q.; Li, Y.; Zhang, G. Two-dimensional MXene-based and MXene-derived photocatalysts: Recent developments and perspectives. *Chem. Eng. J.* **2021**, *409*, 128099. [CrossRef]
33. Sharma, V.; Kumar, A.; Kumar, A.; Krishnan, V. Enhanced photocatalytic activity of two dimensional ternary nanocomposites of ZnO-Bi_2WO_6-Ti_3C_2 MXene under natural sunlight irradiation. *Chemosphere* **2022**, *287*, 132119. [CrossRef] [PubMed]
34. Yang, C.; Tan, Q.; Li, Q.; Zhou, J.; Fan, J.; Li, B.; Sun, J.; Lv, K. 2D/2D Ti_3C_2 MXene/g-C_3N_4 nanosheets heterojunction for high efficient CO_2 reduction photocatalyst: Dual effects of urea. *Appl. Catal. B Environ.* **2020**, *268*, 118738. [CrossRef]
35. Zhou, Y.; Yu, M.; Zhan, R.; Wang, X.; Peng, G.; Niu, J. Ti_3C_2 MXene-induced interface electron separation in g-C_3N_4/Ti_3C_2 MXene/$MoSe_2$ Z-scheme heterojunction for enhancing visible light-irradiated enoxacin degradation. *Sep. Purif. Technol.* **2021**, *275*, 119194. [CrossRef]
36. Cao, S.; Shen, B.; Tong, T.; Fu, J.; Yu, J. 2D/2D Heterojunction of Ultrathin MXene/Bi_2WO_6 Nanosheets for Improved Photocatalytic CO_2 Reduction. *Adv. Funct. Mater.* **2018**, *28*, 1800136. [CrossRef]
37. Wan, L.; Tang, Y.; Chen, L.; Wang, K.; Zhang, J.; Gao, Y.; Lee, J.Y.; Lu, T.; Xu, X.; Li, J.; et al. In-situ construction of g-C_3N_4/Mo_2CT_x hybrid for superior lithium storage with significantly improved Coulombic efficiency and cycling stability. *Chem. Eng. J.* **2021**, *410*, 128349. [CrossRef]
38. Zou, X.; Zhao, X.; Zhang, J.; Lv, W.; Qiu, L.; Zhang, Z. Photocatalytic degradation of ranitidine and reduction of nitrosamine dimethylamine formation potential over MXene-Ti_3C_2/MoS_2 under visible light irradiation. *J. Hazard Mater.* **2021**, *413*, 125424. [CrossRef]
39. Chen, X.; Guo, Y.; Bian, R.; Ji, Y.; Wang, X.; Zhang, X.; Cui, H.; Tian, J. Titanium carbide MXenes coupled with cadmium sulfide nanosheets as two-dimensional/two-dimensional heterostructures for photocatalytic hydrogen production. *J. Colloid Interface Sci.* **2022**, *613*, 644–651. [CrossRef]
40. Cui, C.; Guo, R.; Xiao, H.; Ren, E.; Song, Q.; Xiang, C.; Lai, X.; Lan, J.; Jiang, S. Bi_2WO_6/Nb_2CT_x MXene hybrid nanosheets with enhanced visible-light-driven photocatalytic activity for organic pollutants degradation. *Appl. Surf. Sci.* **2020**, *505*, 144595. [CrossRef]
41. Li, J.; Wang, S.; Du, Y.; Liao, W. Enhanced photocatalytic performance of TiO_2@C nanosheets derived from two-dimensional Ti_2CT_x. *Ceram. Int.* **2018**, *44*, 7042–7046. [CrossRef]
42. Li, J.; Du, Y.; Huo, C.; Wang, S.; Cui, C. Thermal stability of two-dimensional Ti_2C nanosheets. *Ceram. Int.* **2015**, *41*, 2631–2635. [CrossRef]
43. Ahmed, B.; Anjum, D.H.; Hedhili, M.N.; Gogotsi, Y.; Alshareef, H.N. H_2O_2 assisted room temperature oxidation of Ti_2C MXene for Li-ion battery anodes. *Nanoscale* **2016**, *8*, 7580–7587. [CrossRef]
44. Tran, N.M.; Ta, Q.T.H.; Noh, J.-S. Unusual synthesis of safflower-shaped TiO_2/Ti_3C_2 heterostructures initiated from two-dimensional Ti_3C_2 MXene. *Appl. Surf. Sci.* **2021**, *538*, 148023. [CrossRef]
45. Gong, J.; Li, Y.; Zhao, Y.; Wu, X.; Wang, J.; Zhang, G. Metal-free polymeric (SCN)(n) photocatalyst with adjustable bandgap for efficient organic pollutants degradation and Cr(VI) reduction under visible-light irradiation. *Chem. Eng. J.* **2020**, *402*, 126147. [CrossRef]
46. Zhao, Y.; Li, L.; Zuo, Y.; He, G.; Chen, Q.; Meng, Q.; Chen, H. Reduced graphene oxide supported ZnO/CdS heterojunction enhances photocatalytic removal efficiency of hexavalent chromium from aqueous solution. *Chemosphere* **2022**, *286*, 131738. [CrossRef]

47. Zhao, Y.; Zuo, Y.; He, G.; Chen, Q.; Meng, Q.; Chen, H. Synthesis of graphene-based CdS@CuS core-shell nanorods by cation-exchange for efficient degradation of ciprofloxacin. *J. Alloys Compd.* **2021**, *869*, 159305. [CrossRef]
48. Peng, C.; Xu, W.; Wei, P.; Liu, M.; Guo, L.; Wu, P.; Zhang, K.; Cao, Y.; Wang, H.; Yu, H.; et al. Manipulating photocatalytic pathway and activity of ternary $Cu_2O/(001)TiO_2@Ti_3C_2T_x$ catalysts for H-2 evolution: Effect of surface coverage. *Int. J. Hydrogen Energy* **2019**, *44*, 29975–29985. [CrossRef]
49. Boningari, T.; Inturi, S.N.R.; Suidan, M.; Smirniotis, P.G. Novel continuous single-step synthesis of nitrogen-modified TiO_2 by flame spray pyrolysis for photocatalytic degradation of phenol in visible light. *J. Mater. Sci. Technol.* **2018**, *34*, 1494–1502. [CrossRef]
50. Li, X.; Bai, Y.; Shi, X.; Su, N.; Nie, G.; Zhang, R.; Nie, H.; Ye, L. Applications of MXene ($Ti_3C_2T_x$) in photocatalysis: A review. *Mater. Adv.* **2021**, *2*, 1570–1594. [CrossRef]
51. Wang, H.; Chen, L.; Sun, Y.; Yu, J.; Zhao, Y.; Zhan, X.; Shi, H. Ti_3C_2 Mxene modified $SnNb_2O_6$ nanosheets Schottky photocatalysts with directed internal electric field for tetracycline hydrochloride removal and hydrogen evolution. *Sep. Purif. Technol.* **2021**, *265*, 118516. [CrossRef]
52. Shao, B.; Liu, Z.; Zeng, G.; Liu, Y.; Liang, Q.; He, Q.; Wu, T.; Pan, Y.; Huang, J.; Peng, Z.; et al. Synthesis of 2D/2D CoAl-LDHs/$Ti_3C_2T_x$ Schottky-junction with enhanced interfacial charge transfer and visible-light photocatalytic performance. *Appl. Catal. B Environ.* **2021**, *286*, 119867. [CrossRef]
53. Wang, S.; Lu, A.; Zhong, C.-J. Hydrogen production from water electrolysis: Role of catalysts. *Nano Converg.* **2021**, *8*, 4. [CrossRef] [PubMed]
54. Wang, M.; Yang, H.; Shi, J.; Chen, Y.; Zhou, Y.; Wang, L.; Di, S.; Zhao, X.; Zhong, J.; Cheng, T.; et al. Alloying Nickel with Molybdenum Significantly Accelerates Alkaline Hydrogen Electrocatalysis. *Angew. Chem. Int. Ed.* **2021**, *60*, 5771–5777. [CrossRef] [PubMed]
55. Liu, Y.; Cheng, H.; Cheng, M.; Liu, Z.; Huang, D.; Zhang, G.; Shao, B.; Liang, Q.; Luo, S.; Wu, T.; et al. The application of Zeolitic imidazolate frameworks (ZIFs) and their derivatives based materials for photocatalytic hydrogen evolution and pollutants treatment. *Chem. Eng. J.* **2021**, *417*, 127914. [CrossRef]
56. Yu, Z.-Y.; Duan, Y.; Feng, X.-Y.; Yu, X.; Gao, M.-R.; Yu, S.-H. Clean and Affordable Hydrogen Fuel from Alkaline Water Splitting: Past, Recent Progress, and Future Prospects. *Adv. Mater.* **2021**, *33*, e2007100. [CrossRef] [PubMed]
57. Wang, T.-X.; Liang, H.-P.; Anito, D.A.; Ding, X.; Han, B.-H. Emerging applications of porous organic polymers in visible-light photocatalysis. *J. Mater. Chem. A* **2020**, *8*, 7003–7034. [CrossRef]
58. Jin, H.; Fan, C.; Wei, W.; Zhang, D.; Sun, J.; Cao, C. Evolution of pore structure and produced gases of Zhundong coal particle during gasification in supercritical water. *J. Supercrit. Fluids* **2018**, *136*, 102–109. [CrossRef]
59. Sun, J.; Feng, H.; Kou, J.; Jin, H.; Chen, Y.; Guo, L. Experimental investigation on carbon microstructure for coal gasification in supercritical water. *Fuel* **2021**, *306*, 121675. [CrossRef]
60. Wang, H.-F.; Chen, L.; Pang, H.; Kaskel, S.; Xu, Q. MOF-derived electrocatalysts for oxygen reduction, oxygen evolution and hydrogen evolution reactions. *Chem. Soc. Rev.* **2020**, *49*, 1414–1448. [CrossRef]
61. Wu, H.; Feng, C.; Zhang, L.; Zhang, J.; Wilkinson, D.P. Non-noble Metal Electrocatalysts for the Hydrogen Evolution Reaction in Water Electrolysis. *Electrochem. Energy Rev.* **2021**, *4*, 473–507. [CrossRef]
62. Chen, R.; Wang, Y.; Ma, Y.; Mal, A.; Gao, X.-Y.; Gao, L.; Qiao, L.; Li, X.-B.; Wu, L.-Z.; Wang, C. Rational design of isostructural 2D porphyrin-based covalent organic frameworks for tunable photocatalytic hydrogen evolution. *Nat. Commun.* **2021**, *12*, 1354. [CrossRef] [PubMed]
63. Wang, H.; Lee, J.-M. Recent advances in structural engineering of MXene electrocatalysts. *J. Mater. Chem. A* **2020**, *8*, 10604–10624. [CrossRef]
64. You, J.; Zhao, Y.; Wang, L.; Bao, W. Recent developments in the photocatalytic applications of covalent organic frameworks: A review. *J. Clean. Prod.* **2021**, *291*, 125822. [CrossRef]
65. Ren, Y.; Li, Z.; Deng, B.; Ye, C.; Zhang, L.; Wang, Y.; Li, T.; Liu, Q.; Cui, G.; Asiri, A.M.; et al. Superior hydrogen evolution electrocatalysis enabled by CoP nanowire array on graphite felt. *Int. J. Hydrogen Energy* **2022**, *47*, 3580–3586. [CrossRef]
66. Zhang, Y.; Shi, J.; Huang, Z.; Guan, X.; Zong, S.; Cheng, C.; Zheng, B.; Guo, L. Synchronous construction of CoS_2 in-situ loading and S doping for g-C_3N_4: Enhanced photocatalytic H-2-evolution activity and mechanism insight. *Chem. Eng. J.* **2020**, *401*, 126135. [CrossRef]
67. Samal, R.; Mane, P.; Ratha, S.; Chakraborty, B.; Rout, C.S. Rational Design of Dynamic Bimetallic $NiCoSe_2$/2D $Ti_3C_2T_x$ MXene Hybrids for a High-Performance Flexible Supercapacitor and Hydrogen Evolution Reaction. *Energy Fuels* **2022**, *36*, 15066–15079. [CrossRef]
68. Hong, L.-F.; Guo, R.-T.; Yuan, Y.; Ji, X.-Y.; Li, Z.-S.; Lin, Z.-D.; Pan, W.-G. Recent progress of two-dimensional MXenes in photocatalytic applications: A review. *Mater. Today Energy* **2020**, *18*, 100521. [CrossRef]
69. Cao, B.; Wan, S.; Wang, Y.; Guo, H.; Ou, M.; Zhong, Q. Highly-efficient visible-light-driven photocatalytic H_2 evolution integrated with microplastic degradation over MXene/$Zn_xCd_{1-x}S$ photocatalyst. *J. Colloid Interface Sci.* **2022**, *605*, 311–319. [CrossRef]
70. Xie, X.; Zhang, N.; Tang, Z.-R.; Anpo, M.; Xu, Y.-J. $Ti_3C_2T_x$ MXene as a Janus cocatalyst for concurrent promoted photoactivity and inhibited photocorrosion. *Appl. Catal. B Environ.* **2018**, *237*, 43–49. [CrossRef]
71. Chen, Y.; Liu, C.; Guo, S.; Mu, T.; Wei, L.; Lu, Y. CO_2 capture and conversion to value-added products promoted by MXene-based materials. *Green Energy Environ.* **2022**, *7*, 394–410. [CrossRef]

72. Sharma, S.K.; Kumar, A.; Sharma, G.; Vo, D.-V.N.; Garcia-Penas, A.; Moradi, O.; Sillanpaa, M. MXenes based nano-heterojunctions and composites for advanced photocatalytic environmental detoxification and energy conversion: A review. *Chemosphere* **2022**, *291*, 132923. [CrossRef] [PubMed]
73. Park, Y.H.; Murali, G.; Modigunta, J.K.R.; In, I.; In, S.-I. Recent Advances in Quantum Dots for Photocatalytic CO_2 Reduction: A Mini-Review. *Front. Chem.* **2021**, *9*, 734108. [CrossRef] [PubMed]
74. Biswal, L.; Nayak, S.; Parida, K. Recent progress on strategies for the preparation of 2D/2D MXene/g-C_3N_4 nanocomposites for photocatalytic energy and environmental applications. *Catal. Sci. Technol.* **2021**, *11*, 1222–1248. [CrossRef]
75. Li, J.; Wang, Z.; Chen, H.; Zhang, Q.; Hu, H.; Liu, L.; Ye, J.; Wang, D. A surface-alkalinized Ti_3C_2 MXene as an efficient cocatalyst for enhanced photocatalytic CO_2 reduction over ZnO. *Catal. Sci. Technol.* **2021**, *11*, 4953–4961. [CrossRef]
76. Tang, Q.; Sun, Z.; Deng, S.; Wang, H.; Wu, Z. Decorating g-C_3N_4 with alkalinized Ti_3C_2 MXene for promoted photocatalytic CO_2 reduction performance. *J. Colloid Interface Sci.* **2020**, *564*, 406–417. [CrossRef] [PubMed]
77. Ding, M.; Han, C.; Yuan, Y.; Xu, J.; Yang, X. Advances and Promises of 2D MXenes as Cocatalysts for Artificial Photosynthesis. *Sol. RRL* **2021**, *5*, 2100603. [CrossRef]
78. Sun, B.; Qiu, P.; Liang, Z.; Xue, Y.; Zhang, X.; Yang, L.; Cui, H.; Tian, J. The fabrication of 1D/2D CdS nanorod@Ti_3C_2 MXene composites for good photocatalytic activity of hydrogen generation and ammonia synthesis. *Chem. Eng. J.* **2021**, *406*, 127177. [CrossRef]
79. Shen, Z.K.; Yuan, Y.J.; Wang, P.; Bai, W.; Pei, L.; Wu, S.; Yu, Z.T.; Zou, Z. Few-Layer Black Phosphorus Nanosheets: A Metal-Free Cocatalyst for Photocatalytic Nitrogen Fixation. *ACS Appl. Mater. Interfaces* **2020**, *12*, 17343–17352. [CrossRef]
80. Kok, S.H.W.; Lee, J.; Tan, L.-L.; Ong, W.-J.; Chai, S.-P. MXene-A New Paradigm Toward Artificial Nitrogen Fixation for Sustainable Ammonia Generation: Synthesis, Properties, and Future Outlook. *Acs Mater. Lett.* **2022**, *4*, 212–245. [CrossRef]
81. Fang, Y.; Cao, Y.; Tan, B.; Chen, Q. Oxygen and Titanium Vacancies in a BiOBr/MXene-Ti_3C_2 Composite for Boosting Photocatalytic N-2 Fixation. *ACS Appl. Mater. Interfaces* **2021**, *13*, 42624–42634. [CrossRef]
82. Hao, C.; Liao, Y.; Wu, Y.; An, Y.; Lin, J.; Gu, Z.; Jiang, M.; Hu, S.; Wang, X. RuO_2-loaded TiO_2-MXene as a high performance photocatalyst for nitrogen fixation. *J. Phys. Chem. Solids* **2020**, *136*, 109141. [CrossRef]
83. Chen, X.; Li, Y.; Wu, Z.; Xu, X.; Zhu, W.; Gao, X. $Bi_4O_5Br_2$ anchored on Ti_3C_2 MXene with ohmic heterojunction in photocatalytic NH_3 production: Insights from combined experimental and theoretical calculations. *J. Colloid Interface Sci.* **2021**, *602*, 553–562. [CrossRef]
84. Hou, T.; Li, Q.; Zhang, Y.; Zhu, W.; Yu, K.; Wang, S.; Xu, Q.; Liang, S.; Wang, L. Near-infrared light-driven photofixation of nitrogen over $Ti_3C_2T_x/TiO_2$ hybrid structures with superior activity and stability. *Appl. Catal. B Environ.* **2020**, *273*, 119072. [CrossRef]
85. Gao, W.; Li, X.; Luo, S.; Luo, Z.; Zhang, X.; Huang, R.; Luo, M. In situ modification of cobalt on MXene/TiO_2 as composite photocatalyst for efficient nitrogen fixation. *J. Colloid Interface Sci.* **2021**, *585*, 20–29. [CrossRef]
86. Peng, C.; Yang, X.; Li, Y.; Yu, H.; Wang, H.; Peng, F. Hybrids of Two-Dimensional Ti_3C_2 and TiO_2 Exposing {001} Facets toward Enhanced Photocatalytic Activity. *ACS Appl. Mater. Interfaces* **2016**, *8*, 6051–6060. [CrossRef] [PubMed]
87. Tang, R.; Xiong, S.; Gong, D.; Deng, Y.; Wang, Y.; Su, L.; Ding, C.; Yang, L.; Liao, C. Ti_3C_2 2D MXene: Recent Progress and Perspectives in Photocatalysis. *ACS Appl. Mater. Interfaces* **2020**, *12*, 56663–56680. [CrossRef] [PubMed]
88. Lai, Y.-J.; Lee, D.-J. Solid mediator Z-scheme heterojunction photocatalysis for pollutant oxidation in water: Principles and synthesis perspectives. *J. Taiwan Inst. Chem. Eng.* **2021**, *125*, 88–114. [CrossRef]
89. Wu, F.-D.; Chen, J.-C.; Hu, J.-P. Synthesis of $TiO_2/Ti_3C_2T_x$/AgI Z-scheme photocatalyst for tetracycline hydrochloride photocatalytic degradation. *J. Environ. Chem. Eng.* **2022**, *10*, 107117. [CrossRef]
90. Tian, P.; He, X.; Zhao, L.; Li, W.; Fang, W.; Chen, H.; Zhang, F.; Huang, Z.; Wang, H. Enhanced charge transfer for efficient photocatalytic H_2 evolution over UiO-66-NH_2 with annealed $Ti_3C_2T_x$ MXenes. *Int. J. Hydrogen Energy* **2019**, *44*, 788–800. [CrossRef]
91. Yang, J.-X.; Yu, W.-B.; Li, C.-F.; Dong, W.-D.; Jiang, L.-Q.; Zhou, N.; Zhuang, Z.-P.; Liu, J.; Hu, Z.-Y.; Zhao, H.; et al. PtO nanodots promoting Ti_3C_2 MXene in-situ converted Ti_3C_2/TiO_2 composites for photocatalytic hydrogen production. *Chem. Eng. J.* **2021**, *420*, 129695. [CrossRef]
92. Yang, W.; Ma, G.; Fu, Y.; Peng, K.; Yang, H.; Zhan, X.; Yang, W.; Wang, L.; Hou, H. Rationally designed Ti_3C_2 MXene@$TiO_2/CuInS_2$ Schottky/S-scheme integrated heterojunction for enhanced photocatalytic hydrogen evolution. *Chem. Eng. J.* **2022**, *429*, 132381. [CrossRef]
93. Su, T.; Hood, Z.D.; Naguib, M.; Bai, L.; Luo, S.; Rouleau, C.M.; Ivanov, I.N.; Ji, H.; Qin, Z.; Wu, Z. Monolayer $Ti_3C_2T_x$ as an Effective Co-catalyst for Enhanced Photocatalytic Hydrogen Production over TiO_2. *ACS Appl. Energy Mater.* **2019**, *2*, 4640–4651. [CrossRef]
94. Liu, Y.; Li, Y.H.; Li, X.; Zhang, Q.; Yu, H.; Peng, X.; Peng, F. Regulating Electron-Hole Separation to Promote Photocatalytic H_2 Evolution Activity of Nanoconfined Ru/MXene/TiO_2 Catalysts. *ACS Nano* **2020**, *14*, 14181–14189. [CrossRef] [PubMed]
95. Li, Y.; Li, W.; Zhou, Q. Haploid pluripotent stem cells: Twofold benefits with half the effort in genetic screening and reproduction. *Curr. Opin. Genet. Dev.* **2020**, *64*, 6–12. [CrossRef]
96. Yuan, W.; Cheng, L.; An, Y.; Lv, S.; Wu, H.; Fan, X.; Zhang, Y.; Guo, X.; Tang, J. Laminated Hybrid Junction of Sulfur-Doped TiO_2 and a Carbon Substrate Derived from Ti_3C_2 MXenes: Toward Highly Visible Light-Driven Photocatalytic Hydrogen Evolution. *Adv. Sci.* **2018**, *5*, 1700870. [CrossRef] [PubMed]

97. Li, Y.; Deng, X.; Tian, J.; Liang, Z.; Cui, H. Ti_3C_2 MXene-derived Ti_3C_2/TiO_2 nanoflowers for noble-metal-free photocatalytic overall water splitting. *Appl. Mater. Today* **2018**, *13*, 217–227. [CrossRef]
98. Li, Y.; Yin, Z.; Ji, G.; Liang, Z.; Xue, Y.; Guo, Y.; Tian, J.; Wang, X.; Cui, H. 2D/2D/2D heterojunction of Ti_3C_2 MXene/MoS_2 nanosheets/TiO_2 nanosheets with exposed (001) facets toward enhanced photocatalytic hydrogen production activity. *Appl. Catal. B Environ.* **2019**, *246*, 12–20. [CrossRef]
99. Makola, L.C.; Moeno, S.; Ouma, C.N.M.; Sharma, A.; Vo, D.-V.N.; Dlamini, L.N. Facile fabrication of a metal-free 2D–2D Nb_2CT_x@g-C_3N_4 MXene-based Schottky-heterojunction with the potential application in photocatalytic processes. *J. Alloys Compd.* **2022**, *916*, 165459. [CrossRef]
100. Huang, J.; Tao, J.; Liu, G.; Lu, L.; Tang, H.; Qiao, G. In situ construction of 1D CdS/2D Nb_2CT_x MXene Schottky heterojunction for enhanced photocatalytic hydrogen production activity. *Appl. Surf. Sci.* **2022**, *573*, 151491. [CrossRef]
101. Zuo, G.; Wang, Y.; Teo, W.L.; Xie, A.; Guo, Y.; Dai, Y.; Zhou, W.; Jana, D.; Xian, Q.; Dong, W.; et al. Ultrathin $ZnIn_2S_4$ Nanosheets Anchored on $Ti_3C_2T_x$ MXene for Photocatalytic H_2 Evolution. *Angew. Chem. Int. Ed.* **2020**, *59*, 11287–11292. [CrossRef]
102. Zhang, Z.; Yates, J.T., Jr. Band Bending in Semiconductors: Chemical and Physical Consequences at Surfaces and Interfaces. *Chem. Rev.* **2012**, *112*, 5520–5551. [CrossRef] [PubMed]
103. Lin, J.; Yu, Y.; Zhang, Z.; Gao, F.; Liu, S.; Wang, W.; Li, G. A Novel Approach for Achieving High-Efficiency Photoelectrochemical Water Oxidation in InGaN Nanorods Grown on Si System: MXene Nanosheets as Multifunctional Interfacial Modifier. *Adv. Funct. Mater.* **2020**, *30*, 1910479. [CrossRef]
104. Ran, J.; Gao, G.; Li, F.-T.; Ma, T.-Y.; Du, A.; Qiao, S.-Z. Ti_3C_2 MXene co-catalyst on metal sulfide photo-absorbers for enhanced visible-light photocatalytic hydrogen production. *Nat. Commun.* **2017**, *8*, 13907. [CrossRef]
105. Li, L.; Wang, X.; Guo, H.; Yao, G.; Yu, H.; Tian, Z.; Li, B.; Chen, L. Theoretical Screening of Single Transition Metal Atoms Embedded in MXene Defects as Superior Electrocatalyst of Nitrogen Reduction Reaction. *Small Methods* **2019**, *3*, 1900337. [CrossRef]
106. Zhong, T.; Yu, Z.; Jiang, R.; Hou, Y.; Chen, H.; Ding, L.; Lian, C.; Zou, B. Surface-Activated $Ti_3C_2T_x$ MXene Cocatalyst Assembled with CdZnS-Formed 0D/2D CdZnS/Ti_3C_2-A_{40} Schottky Heterojunction for Enhanced Photocatalytic Hydrogen Evolution. *Sol. RRL* **2021**, *6*, 2100863. [CrossRef]
107. Cai, T.; Wang, L.L.; Liu, Y.T.; Zhang, S.Q.; Dong, W.Y.; Chen, H.; Yi, X.Y.; Yuan, J.L.; Xia, X.N.; Liu, C.B.; et al. Ag_3PO_4/Ti_3C_2 MXene interface materials as a Schottky catalyst with enhanced photocatalytic activities and anti-photocorrosion performance. *Appl. Catal. B Environ.* **2018**, *239*, 545–554. [CrossRef]